A Comparison of Full-Spectrum and Complex-Symbol Combining Techniques for the Galileo S-Band Mission

S. Million, B. Shah, and S. Hinedi
Communications Systems Research Section

Full-spectrum combining (FSC) and complex-symbol combining (CSC) are two antenna-arraying techniques being considered for the Galileo spacecraft's upcoming encounter with Jupiter. This article describes the performance of these techniques in terms of symbol signal-to-noise ratio (SNR) degradation and symbol SNR loss. It is shown that both degradation and loss are approximately equal at low values of symbol SNR but diverge at high SNR values. For the Galileo S-band (2.2 to 2.3 GHz) mission, degradation provides a good estimate of performance as the symbol SNR is typically below −5 dB.

For the following arrays—two 70-m antennas, one 70-m and one 34-m antenna, one 70-m and two 34-m antennas, and one 70-m and three 34-m antennas—it is shown that FSC has less degradation than CSC when the subcarrier and symbol window-loop bandwidth products are above 3.0, 10.0, 8.5, and 8.2 mHz at the symbol rate of 200 sym/sec, and above 1.2, 4.5, 4.0, and 3.5 mHz at a symbol rate of 400 sym/sec, respectively. Moreover, for an array of four 34-m antennas, FSC has less degradation than CSC when the subcarrier and symbol window-loop bandwidth products are above 0.32 mHz at the symbol rate of 50 sym/sec and above 0.8 mHz at the symbol rate of 25 sym/sec.

I. Introduction

In deep-space communications, combining signals from multiple antennas is commonly referred to as arraying. Arraying techniques are important because they can significantly enhance system performance. For example, if signal power-to-noise density ratio (P/N_0) is a measure of system performance, then the effective P/N_0 after arraying ideally should be equal to the sum of the P/N_0's corresponding to individual antennas. A typical array-

ing design trades complexity and gain (or improvement in system performance). Arraying is an attractive option for communication links operating near threshold. For instance, consider the Galileo spacecraft, which is currently on its way to Jupiter. Due to a malfunctioned high-gain antenna, Galileo must rely on its low-gain S-band antenna (and a much reduced link margin) for data transmission to Earth. The Galileo S-band mission will employ arraying, as well as other techniques such as suppressed carriers and data compression, to improve its link margin and maximize data return. The current plan is to implement an intercontinental array between antenna complexes in Australia, Spain, and the United States. Each complex has one 70-m and several 34-m antennas available for arraying. This article compares the full-spectrum combining (FSC) and complex-symbol combining (CSC) arraying techniques for the following five antenna combinations: two 70-m antennas; one 70-m and one 34-m antenna; one 70-m and two 34-m antennas; one 70-m and three 34-m antennas; and four 34-m antennas. Even when communication links are operating above threshold, arraying is an economically attractive option to increase the scientific return of a mission without having to build larger antennas. Smaller, inexpensive antennas (i.e., 34-m) can be built at less cost than a single larger antenna (i.e., 70-m), but with at least an equivalent performance after proper arraying.

A recent study [1], which presented an overview of several antenna-combining techniques, concluded that FSC resulted in the least degradation for weak signals. That study didn't consider the CSC arraying technique, which has been made possible by the advent of all-digital receivers in NASA's Deep Space Network (DSN) [2]. The CSC technique is an attractive arraying option because it requires little modification to existing systems. In FSC, depicted in Fig. 1(a), the received radio frequency (RF) signal at each antenna is downconverted to an intermediate frequency (IF), transmitted to a central location where it is aligned and combined with signals from other antennas, and then demodulated by a single receiver chain. The chain consists of one carrier loop, one subcarrier loop, one symbol-synchronization loop, and one matched filter. The RF/IF downconverter is assumed to output a complex IF signal (two IF signals that are orthogonal) denoted by the double lines in Fig. 1(a). The processing needed to align and combine the IF signals is shown in Fig. 1(b) for an array of two antennas. The details of this scheme are discussed in the section on FSC performance.

In CSC, depicted in Fig. 2(a), the received RF signal at each antenna is first open-loop downconverted to IF; it, in turn, is open-loop downconverted near baseband using a complex IF reference. The IF in-phase (I) and quadra-

ture (Q) references are tuned to the predicted IF carrier frequency. The resulting complex signal near baseband, centered at the carrier predict error, is used for subcarrier tracking and symbol synchronization, which can be accomplished using either the I arm of the carrier alone or both the I and Q arms. The latter requires more complexity but results in an improved performance, as one would expect. After subcarrier demodulation, the signal is input to a pair of matched filters that output soft-quantized complex symbols that modulate a tone with frequency equal to the carrier-predict error. Since there are two channels in the down-conversion process (carriers I and Q), the symbols at the matched filter output modulate quadrature tones and can be viewed as complex symbols. The complex symbols from multiple antennas are then transmitted to a central location, aligned and combined at baseband, and demodulated using a baseband Costas loop. The CSC output is a single real-combined symbol stream. The combiner for CSC is shown in Fig. 2(b) and discussed in the section on CSC performance.

The key difference between FSC and CSC is the order of carrier-phase alignment between the antennas. In FSC, carrier-phase alignment precedes subcarrier demodulation, symbol synchronization, and matched filtering; in CSC, it follows. In both cases, the carrier phases are aligned and the signals are combined prior to carrier phase tracking and demodulation. As a result, for an array of two 70-m antennas, the effective P/N_0 at the input to the subcarrier and symbol loops in CSC is about 6 dB lower than FSC. Three of the 6 dB are due to the signals in CSC being combined after the subcarrier and symbol loops; the remaining 3 dB result from subcarrier and symbol synchronization that is performed without carrier lock.

Assuming the carrier is locked, the effective P/N_0 at the input to the subcarrier and symbol loops in CSC is about 3 dB lower than FSC. Another key difference between FSC and CSC arises when arraying a 70-m and 34-m antenna. In the Galileo case, the signal is so weak that it is harder for a stand-alone 34-m antenna to lock to the signal than a stand-alone 70-m antenna. Consequently, when implementing CSC between the two, the 70-m antenna needs to enable the 34-m antenna in tracking the subcarrier and symbols. When they are located within a few miles of each other, the 70-m antenna can transmit subcarrier and symbol-loop frequency and phase information to the 34-m antenna. However, when implementing FSC between a 70-m and 34-m antenna array, no aiding of the 34-m antenna is required since the carrier, subcarrier, and symbol-timing loops operate on the combined signal. Furthermore, since it is difficult for a single 34-m antenna to lock on to the signal by itself, an array of four 34-m antennas is less effective

using CSC than FSC. These differences are summarized in Table 1.

In this article, the performances of FSC and CSC are measured both in terms of symbol SNR degradation and symbol SNR loss. Symbol SNR degradation is defined as the ratio of the SNR at the matched filter output in the presence of nonideal synchronization to the SNR in the presence of ideal synchronization. On the other hand, symbol SNR loss is defined as the additional symbol SNR needed in the presence of imperfect synchronization to achieve the same symbol error rate (SER) as in the presence of perfect synchronization. Mathematical representations of degradation and loss are given in the next section. Comparatively, loss gives the absolute, while degradation gives the relative, performance advantage of an arraying scheme. Moreover, since the calculation of degradation is less demanding than computation of loss [3], it is the preferred calculation method at low-symbol SNR's where it is approximately equal to loss. In the following sections, the degradation and loss for a single antenna, FSC, and CSC are derived and then illustrated via various numerical examples.

II. Single Receiver Performance

In deep-space communications, the downlink symbols are first modulated onto a square-wave subcarrier; the modulated subcarrier then modulates an RF carrier [4]. This allows transmission of a residual carrier component whose frequency does not coincide with the data spectrum. At the receiver, the deep-space signal is demodulated using a carrier-tracking loop, a subcarrier-tracking loop [5], and a symbol-synchronizer loop [6], as shown in Fig. 3. Depending on the modulation index, carrier tracking can be achieved by a phase-locked loop (PLL), Costas loop, or both [7]. The PLL or a combination of loops is used for modulation indices less than 90 deg, whereas a Costas loop is used when the modulation index is equal to 90 deg. The deep-space signal with the carrier fully suppressed[1] can be represented as [8]

$$r(t) = \sqrt{2P}d(t)\text{Sqr}(\omega_{sc}t + \theta_{sc})\cos{(\omega_c t + \theta_c)} + n(t) \quad (1)$$

where P is the received data power in watts (W); ω_c and θ_c are the carrier angular frequency in radians per second (rads/sec) and phase in rads, respectively; and $\text{Sqr}(\omega_{sc}t + \theta_{sc})$ is the square-wave subcarrier with subcarrier angular

---

[1] This article considers the Galileo S-band scenario in which the carrier is fully suppressed.

frequency ω_{sc} in rads/sec and subcarrier phase θ_{sc} in rads. The symbol stream $d(t)$ is given by

$$d(t) = \sum_{k=-\infty}^{\infty} d_k p(t - kT) \quad (2)$$

where d_k is the ± 1 binary data for the kth symbol and T is the symbol period in seconds. The baseband pulse p(t) is unit power and limited to T seconds. The narrow-band noise $n(t)$ can be written as

$$n(t) = \sqrt{2}n_c(t)\cos{(\omega_c t + \theta_c)} - \sqrt{2}n_s(t)\sin{(\omega_c t + \theta_c)} \quad (3)$$

where $n_c(t)$ and $n_s(t)$ are statistically independent, stationary, band-limited, white Gaussian noise processes with one-sided spectral density level N_0 (W/Hz) and one-sided bandwidth W_n (Hz), which is large compared to 1/T. After signal demodulation, the symbol stream at the output of the matched filter in Fig. 3 can be written as [8]

$$v_k = \begin{cases} \sqrt{P}C_c C_{sc}d_k + n_k & d_k = d_{k-1} \\ \sqrt{P}C_c C_{sc}(1 - \frac{|\phi_{sy}|}{\pi})d_k + n_k & d_k \neq d_{k-1} \end{cases} \quad (4)$$

where the noise n_k is a Gaussian random variable with variance $\sigma_n^2 = N_0/2T$. The signal reduction functions C_c and C_{sc} are due to imperfect carrier and subcarrier synchronization and are given by [1]

$$C_c = \cos{\phi_c} \quad (5)$$

$$C_{sc} = 1 - \frac{2}{\pi}|\phi_{sc}| \quad (6)$$

where ϕ_c and ϕ_{sc} (in rads), respectively, denote the carrier- and subcarrier-phase tracking errors. The symbol timing error ϕ_{sy}, which affects the output only when there is a symbol transition, reduces the signal amplitude by $1 - |\phi_{sy}|/\pi$. Ideally, $\phi_c = \phi_{sc} = \phi_{sy} = 0$ and Eq. (4) reduce to the ideal matched filter output $v_k = \sqrt{P}d_k + n_k$, as expected. In writing Eq. (4), it is assumed that the carrier, subcarrier, and symbol loop bandwidths are much smaller than the symbol rate so that the phase errors ϕ_c, ϕ_{sc}, and ϕ_{sy} can be modeled as constant over several symbols. Throughout this article, ϕ_c is assumed to be Tikhonov distributed, and ϕ_{sc} and ϕ_{sy} are assumed to be Gaussian distributed. Let $p_c(\phi_c)$, $p_{sc}(\phi_{sc})$, and $p_{sy}(\phi_{sy})$ denote respectively the carrier, subcarrier, and symbol phase error density functions. Then

$$p_c(\phi_c) = \begin{cases} \dfrac{\exp\left(\frac{1}{4}\rho_c \cos 2\phi_c\right)}{\pi I_0(\frac{1}{4}\rho_c)} & |\phi_c| \le \frac{\pi}{2} \\ 0 & \text{otherwise} \end{cases} \qquad (7)$$

where $I_k(x)$ denotes the modified Bessel function of order k, and ρ_c is the suppressed carrier or Costas loop SNR. Also, $p_{sc}(\phi_{sc})$ and $p_{sy}(\phi_{sy})$ are given by

$$p_i(\phi_i) = \frac{\exp\left(-\phi_i^2/2\sigma_i^2\right)}{\sqrt{2\pi}\sigma_i}, \quad i = sc,\ sy \qquad (8)$$

where σ_{sc}^2 and σ_{sy}^2 are the reciprocals of the subcarrier and symbol loop SNR's, respectively, denoted as ρ_{sc} and ρ_{sy}. The carrier [8], subcarrier [8], and symbol [6] loop SNR's are respectively given as

$$\rho_c = \frac{P/N_0}{B_c}\left(1 + \frac{1}{2E_s/N_0}\right)^{-1} \qquad (9)$$

$$\rho_{sc} = \left(\frac{2}{\pi}\right)^2 \frac{P/N_0}{W_{sc}B_{sc}}\left(1 + \frac{1}{2E_s/N_0}\right)^{-1} \qquad (10)$$

$$\rho_{sy} = \frac{P/N_0}{2\pi^2 W_{sy}B_{sy}} \frac{\left(\text{erf}\left(\sqrt{\frac{E_s}{N_0}}\right) - \frac{W_{sy}}{2\sqrt{\pi}}\sqrt{\frac{E_s}{N_0}}\exp\left(-\frac{E_s}{N_0}\right)\right)^2}{\left(1 + \frac{E_s}{N_0}\frac{W_{sy}}{2} - \frac{W_{sy}}{2}\left[\frac{1}{\sqrt{\pi}}\exp\left(-\frac{E_s}{N_0}\right) + \sqrt{\frac{E_s}{N_0}}\,\text{erf}\left(\sqrt{\frac{E_s}{N_0}}\right)\right]^2\right)} \qquad (11)$$

where $E_s/N_0 = PT/N_0$ is the symbol SNR, erf $(x) = 2/\sqrt{\pi}\int_0^x \exp\left(-v^2\right) dv$ is the error function, and B_c, B_{sc}, and B_{sy} (in Hz) denote the single-sided carrier, subcarrier, and symbol loop bandwidths, respectively. The parameters W_{sc} and W_{sy}, which denote the subcarrier and symbol window, are unitless and limited to $(0, 1]$. The loop SNR's for the subcarrier and symbol loop are valid only when $\pi/2\ W_{sc} \gtrsim \sigma_{sc}$ and $\pi W_{sy} \gtrsim \sigma_{sy}$.

A useful quantity needed to compute degradation and loss is the symbol SNR conditioned on ϕ_c, ϕ_{sc}, and ϕ_{sy}. The conditional symbol SNR, denoted SNR', is defined as the square of the conditional mean of v_k divided by the conditional variance of v_k, i.e.,

$$SNR' = \frac{\overline{(v_k/\phi_c, \phi_{sc}, \phi_{sy})}^2}{\sigma_n^2}$$

$$= \begin{cases} \dfrac{2PT}{N_0}C_c^2 C_{sc}^2 & d_k = d_{k-1} \\ \dfrac{2PT}{N_0}C_c^2 C_{sc}^2\left(1 - \dfrac{|\phi_{sy}|}{\pi}\right)^2 & d_k \ne d_{k-1} \end{cases} \qquad (12)$$

where $\overline{(x/y)}$ denotes the statistical expectation of x conditioned on y, and v_k and σ_n^2 are defined earlier.

A. Degradation

The symbol SNR degradation is defined as the ratio of the unconditional SNR at the output of the matched filter in the presence of imperfect synchronization to the ideal matched filter output SNR. The unconditional SNR, denoted SNR, is found by first averaging Eq. (12) over the symbol transition probability, and then over the carrier, subcarrier, and symbol phases. Letting $\bar{x}$ denote the average of x, the unconditional SNR is given as

$$SNR = \frac{2PT}{N_0}\overline{C_c^2}\ \overline{C_{sc}^2}\ \overline{C_{sy}^2} \qquad (13)$$

where the signal amplitude reduction due to symbol timing errors (averaged over the symbol transition probability) is denoted C_{sy}, and given as

$$C_{sy} = 1 - \frac{|\phi_{sy}|}{2\pi} \qquad (14)$$

Averaging over the phases yields [1]

$$\overline{C_c^2} = \frac{1}{2}\left[1 + \frac{I_1(\frac{1}{4}\rho_c)}{I_0(\frac{1}{4}\rho_c)}\right]$$ (15)

$$\overline{C_{sc}^2} = 1 - \sqrt{\frac{32}{\pi^3}}\frac{1}{\sqrt{\rho_{sc}}} + \frac{4}{\pi^2}\frac{1}{\rho_{sc}}$$ (16)

$$\overline{C_{sy}^2} = 1 - \sqrt{\frac{2}{\pi^3}}\frac{1}{\sqrt{\rho_{sy}}} + \frac{1}{4\pi^2}\frac{1}{\rho_{sy}}$$ (17)

Ideally, when there are no phase errors (i.e., when $\rho_c = \rho_{sc} = \rho_{sy} = \infty$), $\overline{C_c^2} = \overline{C_{sc}^2} = \overline{C_{sy}^2} = 1$ and Eq. (13) reduce to $SNR_{ideal} = 2PT/N_0$, as expected. The degradation, D, for a single antenna is thus given by

$$D = -10\,\log_{10}\left(\frac{SNR}{SNR_{ideal}}\right) = -10\,\log_{10}\overline{C_c^2}\,\overline{C_{sc}^2}\,\overline{C_{sy}^2}$$ (18)

B. Loss

For the single receiver shown in Fig. 3, the SER, denoted $P_s(E)$, is defined as

$$P_s(E) = \int_{-\frac{\pi}{2}}^{\frac{\pi}{2}}\int_{-\infty}^{\infty}\int_{-\infty}^{\infty} P_s'(E)p_c(\phi_c)p_{sc}(\phi_{sc})p_{sy}(\phi_{sy})$$

$$\times\, d\phi_{sy}d\phi_{sc}d\phi_c = f\left(\sqrt{\frac{E_s}{N_0}}\right)$$ (19)

where $f(\bullet)$ is the functional relationship between SER and $\sqrt{E_s/N_0}$ and $P_s'(E)$ is the SER conditioned on the phase errors ϕ_c, ϕ_{sc}, and ϕ_{sy}. Following similar steps as in [9], the conditional SER can be shown to be

$$P_s'(E) = \frac{1}{4}\,\text{erfc}\left(\sqrt{SNR'\text{ when }d_k \neq d_{k-1}}\right)$$

$$+ \frac{1}{4}\,\text{erfc}\left(\sqrt{SNR'\text{ when }d_k = d_{k-1}}\right)$$ (20)

where

$$\text{erfc}\,(x) = \frac{2}{\sqrt{\pi}}\int_x^{\infty}\exp\left(-v^2\right)dv = 1 - \text{erf}\,(x)$$ (21)

is the complementary error function. Substituting Eq. (12) for SNR' in Eq. (20) yields

$$P_s'(E) = \frac{1}{4}\text{erfc}\left[\sqrt{\frac{E_s}{N_0}}C_cC_{sc}\left(1 - \frac{|\phi_{sy}|}{\pi}\right)\right]$$

$$+ \frac{1}{4}\text{erfc}\left[\sqrt{\frac{E_s}{N_0}}C_cC_{sc}\right]$$ (22)

Ideally, when there are no timing errors (i.e., when $\rho_c = \rho_{sc} = \rho_{sy} = \infty$), $C_c = C_{sc} = (1-|\phi_{sy}|/\pi) = 1$ and Eq. (19) reduce to the well-known binary phase-shift keyed (BPSK) error rate, $P_s(E) = (1/2)\,\text{erfc}\,(\sqrt{E_s/N_0})$.

Symbol SNR loss is defined as the additional symbol SNR needed in the presence of imperfect synchronization to achieve the same SER as in the presence of perfect synchronization. Mathematically, the SNR loss due to imperfect carrier, subcarrier, and symbol timing references is given in dB as

$$L_{dB} = -20\log\left[f^{-1}(P_s(E))\right]\Big|_{\left[\text{infinite loop SNR}\right]}$$

$$+ 20\log\left[f^{-1}(P_s(E))\right]\Big|_{\left[\text{finite loop SNR}\right]}$$ (23)

where $P_s(E)$ is defined in Eq. (19). The first term in Eq. (23) is the value of E_s/N_0 required at a given value of $P_s(E)$ in the presence of perfect synchronization, whereas the second term is the value of E_s/N_0 required for imperfect synchronization. Note that loss defined in this way is a positive number.

III. FSC Performance

The FSC technique, depicted in Fig. 1(a), combines IF signals from multiple antennas and then demodulates the combined signal using the single receiver described in the previous section. The resulting gain is maximized by aligning the IF signals in time and phase prior to demodulation [1]. The alignment algorithm for an array of two antennas is shown in Fig. 1(b). Here signal 1 is assumed to be delayed by τ seconds, with respect to signal 2. The IF signal from antenna 2 is first delayed by $\hat{\tau}$ seconds, where $\hat{\tau}$ can be the output of the delay estimation loop, or it may be predicted from the geometric arrangement of the antennas and spacecraft. After delay compensation, both signals are input to the phase estimator, which outputs $\hat{\theta}_{21}$, the

estimate of θ_{21}, which is the phase of signal 2 relative to signal 1 at the estimator input. Subsequently, signal 2 is phase shifted by an amount equal to $-\hat{\theta}_{21}$, scaled by[2] β_2, and then combined (or added) with signal 1. Notice in Fig. 1(b) that the phase estimator filters the IF signal so that only the L_{sc} harmonics of the IF spectrum are used for phase estimation. It is shown later that the accuracy of the estimates depends on B_{corr}, the bandwidth of the bandpass filter (BPF) centered at IF, and T_c, the estimation period.

The symbol SNR degradation and loss analysis for FSC closely follows the analysis of the previous section as the combined signal is demodulated by a single receiver. As before, imperfect carrier, subcarrier, and symbol synchronization are expected to reduce the symbol SNR. In addition to those effects, however, the reduction due to imperfect combining must be accounted for as well. Assuming that the IF signals in Fig. 1(b) are perfectly aligned in time ($\hat{\tau} = \tau$) but misaligned in phase,[3] the matched filter output for FSC is given by Eq. (4) with the modification that the one-sided noise power spectral density (PSD) level N_0 is now equal to the effective one-sided noise level $N_{0_{eff}}$ of the combined signal, and the data power P is now equal to the combined power P' conditioned on the phase-alignment error. The effective one-sided noise PSD level at the matched filter input is given by [1]

$$N_{0_{eff}} = N_{01} \sum_{n=1}^{L} \gamma_n \qquad (24)$$

where

$$\gamma_n \triangleq \frac{P_n}{P_1} \frac{N_{01}}{N_{0n}} \qquad (25)$$

and where P_n and N_{0n} denote, respectively, the signal power and one-sided noise PSD level of antenna n. Table 2 lists the γ_n factors[4] for several DSN antennas at both S-band (2.2 to 2.3 GHz) and X-band (8.4 to 8.5 GHz). Throughout this article, the ratio P_1/N_{01} is taken to be the signal power to one-sided noise PSD level of the reference antenna which, by convention, is taken to be the antenna

with the highest gain. Consequently, in this article $\gamma_n \leq 1$. Table 2 lists the gamma values for 70-m and 34-m antennas assuming the 70-m antenna is the reference antenna. The same table can be reused for an arbitrary reference antenna as follows. Consider a three-element array consisting of one high-efficiency (HEF) 34-m antenna and two standard (STD) 34-m antennas operating at X-band. Let the 34-m HEF be the reference antenna with $\gamma_1 = 1$, then the 34-m STD antennas have $\gamma_2 = \gamma_3 = 0.13/0.26 = 0.5$.

Let the phase-alignment error between signal n and signal 1 be denoted by $\Delta\phi_{n1} = \theta_{n1} - \hat{\theta}_{n1}$; then the combined signal power conditioned on $\Delta\phi_{n1}$ is given as [1]

$$P' = P_1 \sum_{n=1}^{L} \sum_{m=1}^{L} \gamma_n \gamma_m C_{nm} \qquad (26)$$

where

$$C_{nm} = e^{j(\Delta\phi_{n1} - \Delta\phi_{m1})} \qquad (27)$$

is the complex signal-reduction function due to phase misalignment. To summarize, the matched filter output of FSC is given by Eq. (4) after replacing P by P' as given by Eq. (26) and replacing N_0 by $N_{0_{eff}}$ which is given by Eq. (24).

A useful quantity needed in later calculations is $\overline{C_{nm}}$. In Eq. (27), assuming the residual phase error for each antenna pair, $\Delta\phi_{n1}$ for $n = 2, ..., L$, to be Gaussian distributed with zero mean and variance $\sigma^2_{\Delta\phi_{n1}}$ and statistically independent from $\Delta\phi_{m1}$ for $n \neq m$, then it can be shown that [1]

$$\overline{C_{nm}} = \begin{cases} e^{-\frac{1}{2}[\sigma^2_{\Delta\phi_{n1}} + \sigma^2_{\Delta\phi_{m1}}]} & n \neq m \\ 1 & n = m \end{cases} \qquad (28)$$

where the variance of the residual phase error can be related to the SNR of the correlator as follows:

$$\sigma^2_{\Delta\phi_{n1}} = \frac{1}{2SNR_{n1,fsc}} \qquad (29)$$

Here, $SNR_{n1,fsc}$ denotes correlator SNR [or SNR of the complex signal $\tilde{x}$ in Fig. 1(b)], and it is shown in Appendix A to equal

---

[2] Here, $\beta_2 \triangleq \sqrt{(P_2/P_1)}(N_{01}/N_{02})$ is the weighting factor [3].

[3] This is a simplifying assumption consistent with the assumption in [1].

[4] *Deep Space Network/Flight Project Interface Design Handbook*, D-810-5, Rev. D, vol. I (internal document), Jet Propulsion Laboratory, Pasadena, California, Modules TCI-10, TCI-30, and TLM-10, 1988.

$$SNR_{n1,fsc} \triangleq \frac{E(\tilde{x})E(\tilde{x}^*)}{Var(\tilde{x})} = \frac{E(\tilde{x})E(\tilde{x}^*)}{E(\tilde{x}\tilde{x}^*) - E(\tilde{x})E(\tilde{x}^*)} \quad (30)$$

$$= \frac{T_c(\frac{4}{\pi})^2 \frac{P_1}{N_{01}} \left[\sum\limits_{\substack{j=1 \\ j:odd}}^{L_{sc}} \frac{1}{j^2} \right]}{1 + \frac{1}{\gamma_n} + 2(\frac{\pi}{4})^2 B_{corr} \frac{1}{\sum\limits_{\substack{j=1 \\ j:odd}}^{L_{sc}} \frac{1}{j^2}} \frac{N_{0n}}{P_n}} \quad (31)$$

where B_{corr} is the single-sided bandwidth of the IF filter preceeding the correlator, T_c is the averaging time of the correlator, and L_{sc} is the number of subcarrier harmonics at the BPF output. Note that if all the subcarrier harmonics pass unfiltered, then $\lim_{L_{sc} \to \infty} \sum_{j=1, j:odd}^{L_{sc}} 1/j^2 = 2(\pi/4)^2$.

The SNR conditioned on ϕ_c, ϕ_{sc}, ϕ_{sy}, $\Delta\phi_{n1}$ denoted SNR'_{fsc}, is defined as before to be the square of the conditional mean of v_k divided by the conditional variance of v_k, i.e.,

$$SNR'_{fsc} = \begin{cases} \dfrac{2P_1 T}{N_{01}} C_c^2 C_{sc}^2 \left(\dfrac{\sum\limits_{n=1}^{L} \gamma_n^2 + \sum\limits_{n=1}^{L} \sum\limits_{\substack{m=1 \\ n \neq m}}^{L} \gamma_n \gamma_m C_{nm}}{\sum\limits_{n=1}^{L} \gamma_n} \right) & d_k = d_{k-1} \\[3em] \dfrac{2P_1 T}{N_{01}} C_c^2 C_{sc}^2 \left(1 - \dfrac{|\phi_{sy}|}{\pi} \right)^2 \left(\dfrac{\sum\limits_{n=1}^{L} \gamma_n^2 + \sum\limits_{n=1}^{L} \sum\limits_{\substack{m=1 \\ n \neq m}}^{L} \gamma_n \gamma_m C_{nm}}{\sum\limits_{n=1}^{L} \gamma_n} \right) & d_k \neq d_{k-1} \end{cases} \quad (32)$$

Comparing Eq. (32) with the single receiver conditional SNR in Eq. (12), it is clear that the term inside the large parentheses in Eq. (32) represents the less-than-ideal gain that results from phase misalignment of the IF signals prior to combining.

A. Degradation

The FSC SNR degradation is defined as the unconditional FSC SNR divided by the ideal SNR. The unconditional SNR is found by averaging Eq. (32) over the phases ϕ_c, ϕ_{sc}, ϕ_{sy}, and $\Delta\phi_{n1}$ and is given as

$$SNR_{fsc} = \frac{2P_1 T}{N_{01}} \overline{C_c^2} \; \overline{C_{sc}^2} \; \overline{C_{sy}^2} \left(\frac{\sum\limits_{n=1}^{L} \gamma_n^2 + \sum\limits_{n=1}^{L} \sum\limits_{\substack{m=1 \\ n \neq m}}^{L} \gamma_n \gamma_m \overline{C_{nm}}}{\sum\limits_{n=1}^{L} \gamma_n} \right) \quad (33)$$

where $\overline{C_{nm}}$ is provided in Eq. (28). The quantities $\overline{C_c^2}$, $\overline{C_{sc}^2}$, and $\overline{C_{sy}^2}$ are given in Eqs. (15)–(17) with the modification that the loop SNR's ρ_c, ρ_{sc}, and ρ_{sy} presented in Eqs. (9)–(11) are now computed using the average combined power $P'/N_{0_{eff}}$, which is found by averaging Eq. (26) over the phase $\Delta\phi_{n1}$ and dividing by the effective noise level in Eq. (24). Ideally, when there are no phase errors, $\overline{C_c^2} = \overline{C_{sc}^2} = \overline{C_{sy}^2} = \overline{C_{nm}} = 1$ and Eq. (33) reduce to $\left(2P_1 T/N_{01} \sum_{n=1}^{L} \gamma_n \right)$. Dividing Eq. (33) by the ideal FSC SNR yields the degradation in dB, namely,

$$D_{fsc} = -10 \, \log_{10} \left(\overline{C_c^2} \, \overline{C_{sc}^2} \, \overline{C_{sy}^2} \left(\frac{\left(\sum\limits_{n=1}^{L} \gamma_n^2 + \sum\limits_{n=1}^{L} \sum\limits_{\substack{m=1 \\ n \neq m}}^{L} \gamma_n \gamma_m \overline{C_{nm}} \right)}{\left(\sum\limits_{n=1}^{L} \gamma_n \right)^2} \right) \right) \tag{34}$$

B. Loss

The FSC SER for an L antenna array, denoted $P_{fsc}(E)$, is defined as

$$P_{fsc}(E) = \int\limits_{-\frac{\pi}{2}}^{\frac{\pi}{2}} \int\limits_{-\infty}^{\infty} \int\limits_{-\infty}^{\infty} \int\limits_{-\infty}^{\infty} P'_{fsc}(E) \left[p_c(\phi_c) p_{sc}(\phi_{sc}) p_{sy}(\phi_{sy}) \left(\prod_{n=2}^{L} p_{\Delta\phi_{n1}}(\Delta\phi_{n1}) \right) \right] d\Delta\phi \, d\phi_{sy} \, d\phi_{sc} \, d\phi_c \tag{35}$$

where $\int_{-\infty}^{\infty}$ is the $(L-1)$-tuple integral over the residual phases $\Delta\phi = (\Delta\phi_{21}, ..., \Delta\phi_{(L-1)1})$. Following similar steps as in the single antenna case, the conditional SER becomes

$$P'_{fsc}(E) = \frac{1}{4} \, \text{erfc} \left[\sqrt{\frac{E_{s1}}{N_{01}} \frac{\left(\sum\limits_{n=1}^{L} \gamma_n^2 + \sum\limits_{n=1}^{L} \sum\limits_{\substack{m=1 \\ n \neq m}}^{L} \gamma_n \gamma_m C_{nm} \right)}{\left(\sum\limits_{n=1}^{L} \gamma_n \right)}} \, C_c C_{sc} \left(1 - \frac{|\phi_{sy}|}{\pi} \right) \right]$$

$$+ \frac{1}{4} \, \text{erfc} \left[\sqrt{\frac{E_{s1}}{N_{01}} \frac{\left(\sum\limits_{n=1}^{L} \gamma_n^2 + \sum\limits_{n=1}^{L} \sum\limits_{\substack{m=1 \\ n \neq m}}^{L} \gamma_n \gamma_m C_{nm} \right)}{\left(\sum\limits_{n=1}^{L} \gamma_n \right)}} \, C_c C_{sc} \right] \tag{36}$$

where $E_{s1}/N_{01} = P_1 T/N_{01}$ is the symbol SNR at antenna 1. Ideally, when there are no phase errors, $C_c = C_{sc} = (1 - |\phi_{sy}|/\pi) = C_{nm} = 1$, and Eq. (35) reduces to $P_{fsc}(E) = (1/2) \, \text{erfc} \left(\sqrt{E_s L/N_0} \right)$ for an array of L antennas of the same size (i.e., when $\gamma_n = 1$ for all n). The symbol SNR loss for FSC is given by Eq. (23) after replacing $P_s(E)$ with $P_{fsc}(E)$, as presented in Eq. (35).

IV. CSC Performance

As depicted in Fig. 2(a), signals from multiple antennas in CSC are open-loop downconverted to baseband, partially demodulated using multiple subcarrier loops, multi-ple symbol loops, and multiple matched filters, then combined and demodulated using a single baseband carrier loop. The subcarrier and symbol loops used for CSC can be the same as those used in FSC, or they can be slightly modified versions that take advantage of both the I and Q components of the baseband signal. CSC implementations with the same loops as those in the FSC would use either the I or Q component of the baseband signal. In either case, the loop SNR's of the subcarrier and symbol loops need to be recomputed as the loop input can no longer be assumed to have carrier lock. Let $\rho^I_{sc_n,csc}$ denote the loop SNR of the nth subcarrier loop when either the I or Q arm is used (i.e., the unmodified loop), and let $\rho^{IQ}_{sc_n,csc}$ denote the subcarrier loop SNR when both the I and Q

arms are used (i.e., the modified loop). Similarly, define $\rho^I_{sy_n,csc}$ and $\rho^{IQ}_{sy_n,csc}$ for the nth symbol loop. Then from Appendix B,

$$\rho^I_{sc_n,csc} = \left(\frac{2}{\pi}\right)^2 \frac{P_n/N_{0n}}{2W_{sc_n}B_{sc_n}} \left(1 + \frac{1}{P_nT/N_{0n}}\right)^{-1} \quad (37)$$

$$\rho^I_{sy_n,csc} = \frac{1}{2\pi^2} \frac{P_n/N_{0n}}{W_{sy_n}B_{sy_n}} \mathcal{L}_I \quad (38)$$

and

$$\rho^{IQ}_{sc_n,csc} = \left(\frac{2}{\pi}\right)^2 \frac{P_n/N_{0n}}{W_{sc_n}B_{sc_n}} \left(1 + \frac{1}{P_nT/N_{0n}}\right)^{-1} \quad (39)$$

$$\rho^{IQ}_{sy_n,csc} = \frac{1}{2\pi^2} \frac{P_n/N_{0n}}{W_{sy_n}B_{sy_n}} \mathcal{L}_{IQ} \quad (40)$$

where $W_{sc_n}B_{sc_n}$ and $W_{sy_n}B_{sy_n}$ are the window-loop bandwidth products of the nth subcarrier and symbol loops, respectively. The squaring loss $\mathcal{L}_I$ for the unmodified loop and $\mathcal{L}_{IQ}$ for the modified loop are defined in Appendix B, Section II. For the Galileo scenario, using the unmodified subcarrier and symbol loop reduces the loop SNR by 6 dB compared to the carrier-locked case, while using both the I and Q arms recovers 3 of the 6 dB. Consequently, since the modified subcarrier and symbol loops result in an improved performance, they will be used in this article when comparing CSC to FSC.[5]

Refering to Fig. 2(a), the combining gain is maximized by aligning the baseband signals in time and phase, prior to combining. The alignment algorithm for an array of two antennas is shown in Fig. 2(a). Here signal 1 is assumed to be delayed by m symbols with respect to signal 2. The signals are time aligned by delaying signal 2 by $\hat{m}$ symbols where $\hat{m}$ is an estimate of m. As in FSC, we assume perfect time alignment so that $\hat{m} = m$. After time alignment, the phase of signal 2 with respect to signal 1 is assumed to be θ_{21} rads. Hence, signal 2 is phase shifted by an amount equal to $-\theta_{21}$, scaled by β_2, and then combined with signal 1.

The analysis of CSC degradation and loss begins with the expression for the output of the matched filter in Fig. 2(a). Note that there are actually $2L$ matched filters

[5] The actual operating bandwidth for the modified and unmodified subcarrier and symbol loops are investigated in Appendix B.

per L antennas because after subcarrier demodulation, a real symbol stream is modulated by I and Q tones near baseband. Using complex notation, the matched-filter output stream corresponding to the kth symbol and the nth antenna, conditioned on ϕ_{sc_n} and ϕ_{sc_n}, can be written as

$$\tilde{v}_{k,n} =$$

$$\begin{cases} \sqrt{P_n}C_{sc_n}d_ke^{[j(\Delta\omega_c t_k + \theta_{n1})]} + \tilde{n}_{k,n} \\ \quad d_k = d_{k-1} \\ \sqrt{P_n}C_{sc_n}\left(1 - \frac{|\phi_{sy_n}|}{\pi}\right)d_ke^{[j(\Delta\omega_c t_k + \theta_{n1})]} + \tilde{n}_{k,n} \\ \quad d_k \neq d_{k-1} \end{cases} \quad (41)$$

where the noise $\tilde{n}_{k,n}$ is a complex Gaussian random variable with variance N_0/T. The subcarrier reduction function, C_{sc_n}, is given by Eq. (6) after replacing ϕ_{sc} by ϕ_{sc_n}, the subcarrier phase error for loop n. In addition, the phase ϕ_{sy_n} denotes the symbol-synchronization phase error for loop n, and θ_{n1} is the phase relative to signal 1, i.e., $\theta_{11} = 0$. The baseband carrier frequency Δf_c or $\Delta\omega_c/2\pi$ is equal to the difference between the predicted and actual IF carrier frequency and is assumed to be much less than the symbol rate, i.e., $\Delta f_c \ll 1/T$. The degradation at the output of the matched filter when the carrier is open-loop downconverted is approximately given as

$$D_{\Delta f_c} = \left(\frac{\sin(\pi\Delta f_c T)}{(\pi\Delta f_c T)}\right)^2 \quad (42)$$

Figure 4 illustrates the matched-filter degradation as a function of $\Delta f_c T$, and it is clear that the degradation is less than 0.013 dB when $\Delta f_c T < 0.03$.

The combined signal after phase compensation, $\tilde{z}_k$ in Fig. 2(a), is given as

$$\tilde{z}_k = \sum_{n=1}^{L} \beta_n \tilde{v}_{k,n} e^{-j\hat{\theta}_{n1}} \quad (43)$$

where $\tilde{v}_{k,n}$ is given in Eq. (41) and $\hat{\theta}_{n1}$ is an estimate of θ_{n1}. The optimum combiner weights are given as [3]

$$\beta_n = \sqrt{\frac{P_n}{P_1} \frac{N_{01}}{N_{0n}}} \quad (44)$$

After substituting Eq. (41) for $\tilde{v}_{k,n}$ in Eq. (43), the combined signal can be rewritten as follows (see Appendix C, Section I):

$$\tilde{z}_k = \sqrt{P'}d_k e^{j(\Delta\omega_c t_k + \theta_{\tilde{z}})} + \tilde{n}_k \tag{45}$$

where the variance of the combined complex noise is given as [3]

$$\sigma_{\tilde{n}}^2 = \frac{N_{01}}{T}\sum_{i=1}^{L}\gamma_i \tag{46}$$

The conditional combined signal power P' is given as

$$P' = \begin{cases} P_1 \sum_{n=1}^{L}\sum_{m=1}^{L}\gamma_n\gamma_m C_{sc_n}C_{sc_m}C_{nm} & d_k = d_{k-1} \\ P_1 \sum_{n=1}^{L}\sum_{m=1}^{L}\gamma_n\gamma_m C_{sc_n}C_{sc_m}\left(1 - \frac{|\phi_{sy_n}|}{\pi}\right)\left(1 - \frac{|\phi_{sy_m}|}{\pi}\right)C_{nm} & d_k \neq d_{k-1} \end{cases} \tag{47}$$

where C_{nm} is given by Eq. (27). The signal $\tilde{z}_k$ is then demodulated using a baseband Costas loop with output equal to $e^{-j(\Delta\omega_c t_k + \hat{\theta}_{\tilde{z}})}$, where $\hat{\theta}_{\tilde{z}}$ is an estimate of $\theta_{\tilde{z}}$. The demodulator output is a real combined symbol stream and can be represented as

$$z_k = \sqrt{P'}C_c d_k + n_k \tag{48}$$

where C_c and P' are respectively given by Eqs. (5) and (47). The noise n_k is a real Gaussian random variable with variance $\sigma_n^2 = 1/2\sigma_{\tilde{n}}^2$ where $\sigma_{\tilde{n}}^2$ is given by Eq. (46). The SNR conditioned on ϕ_c, ϕ_{sc_n}, ϕ_{sy_n}, $\Delta\phi_{n1}$, denoted SNR'_{csc}, is defined as the square of the conditional mean of z_k divided by the conditional variance of z_k, i.e,

$$SNR'_{csc} = \begin{cases} \dfrac{2P_1 T}{N_{01}}C_c^2\left(\dfrac{\sum_{n=1}^{L}\sum_{m=1}^{L}\gamma_n\gamma_m C_{sc_n}C_{sc_m}C_{nm}}{\sum_{n=1}^{L}\gamma_n}\right) & d_k = d_{k-1} \\ \dfrac{2P_1 T}{N_{01}}C_c^2\left(\dfrac{\sum_{n=1}^{L}\sum_{m=1}^{L}\gamma_n\gamma_m C_{sc_n}C_{sc_m}\left(1 - \dfrac{|\phi_{sy_n}|}{\pi}\right)\left(1 - \dfrac{|\phi_{sy_m}|}{\pi}\right)C_{nm}}{\sum_{n=1}^{L}\gamma_n}\right) & d_k \neq d_{k-1} \end{cases} \tag{49}$$

The last equation is useful in computing the symbol SNR degradation and loss for CSC as shown below.

A. Degradation

As before, the degradation is found by dividing the unconditional CSC SNR, which includes the effects of synchronization and alignment errors, by the ideal SNR. The unconditional SNR, denoted SNR_{csc}, is computed by taking the statistical expectation of Eq. (49) with respect to ϕ_c, ϕ_{sc_n}, ϕ_{sy_n}, and $\Delta\phi_{n1}$. The phase densities are assumed to be the same as before. In addition, ϕ_{sc_m} and ϕ_{sc_n} are assumed to be independent when $n \neq m$, and the same is true for ϕ_{sy_m} and ϕ_{sy_n}. Consequently,

$$SNR_{csc} = \frac{2P_1 T}{N_{01}} \overline{C_c^2} \frac{\left(\sum_{n=1}^{L} \gamma_n^2 \overline{C_{sc_n}^2} \; \overline{C_{sy_n}^2} + \sum_{n=1}^{L} \sum_{\substack{m=1 \\ n \neq m}}^{L} \gamma_n \gamma_m \overline{C_{sc_n}} \; \overline{C_{sc_m}} \; \overline{C_{sy_n}} \; \overline{C_{sy_m}} \; \overline{C_{nm}} \right)}{\sum_{n=1}^{L} \gamma_n} \tag{50}$$

where the average signal reduction function due to phase misalignment between baseband signals n and m, denoted $\overline{C_{nm}}$, is given by Eq. (28) with $\sigma_{\Delta\phi_{nl}}^2 = 1/(2SNR_{n1,csc})$. The CSC correlator SNR or $SNR_{n1,csc}$ is shown in Appendix C, Section II to be

$$SNR_{n1,csc} = \frac{P_1}{N_{01}} \frac{T_c \overline{C_{sc_1}}^2 \overline{C_{sc_n}}^2 \overline{C_{sy_1}}^2 \overline{C_{sy_n}}^2}{\overline{C_{sc_n}^2} \; \overline{C_{sy_n}^2} + \overline{C_{sc_1}^2} \; \overline{C_{sy_1}^2}(\frac{1}{\gamma_n}) + \frac{N_{0n}}{P_n T}} \tag{51}$$

where T_c is the averaging time of the correlator and T is the symbol period. The loop reduction functions $\overline{C_{sc_n}^2}$ and $\overline{C_{sy_n}^2}$ for the nth subcarrier and symbol loops are respectively given by Eqs. (16) and (17) where the loop SNR's are given by Eqs. (39) and (40). Similarly, $\overline{C_{sc_n}}$ and $\overline{C_{sy_n}}$ can be computed using the same loop SNR as follows [1]:

$$\overline{C_{sc_n}} = 1 - \sqrt{\frac{8}{\pi^3} \frac{1}{\sqrt{\rho_{sc_n}}}} \tag{52}$$

$$\overline{C_{sy_n}} = 1 - \sqrt{\frac{1}{2\pi^3} \frac{1}{\sqrt{\rho_{sy_n}}}} \tag{53}$$

The carrier loop degradation $\overline{C_c^2}$ is given by Eq. (15), with the loop SNR ρ_c computed using the average combined power $P'/N_{0_{eff}}$, which is found by averaging Eq. (47) over all the phases and then dividing by the effective noise level, $N_{0_{eff}} = T\sigma_{\bar{n}}^2$. Ideally, when there are no phase errors, $\overline{C_c^2} = \overline{C_{sc}^2} = \overline{C_{sy}^2} = \overline{C_{sc}} = \overline{C_{sy}} = \overline{C_{nm}} = 1$ and Eq. (50) reduce to $\left[(2P_1 T/N_{01}) \sum_{n=1}^{L} \gamma_n \right]$ as expected. Degradation is defined as before and given as

$$D_{csc} = -10 \, \log_{10} \left(\overline{C_c^2} \left(\frac{\sum_{n=1}^{L} \gamma_n^2 \overline{C_{sc_n}^2} \; \overline{C_{sy_n}^2} + \sum_{n=1}^{L} \sum_{\substack{m=1 \\ n \neq m}}^{L} \gamma_n \gamma_m \overline{C_{sc_n}} \; \overline{C_{sc_m}} \; \overline{C_{sy_n}} \; \overline{C_{sy_m}} \; \overline{C_{nm}}}{\left(\sum_{n=1}^{L} \gamma_i \right)^2} \right) \right) \tag{54}$$

B. Loss

The CSC SER for an L antenna array, denoted $P_{csc}(E)$, is defined as

$$P_{csc}(E) = \int_{-\frac{\pi}{2}}^{\frac{\pi}{2}} \int_{-\infty}^{\infty} \int_{-\infty}^{\infty} \int_{-\infty}^{\infty} P'_{csc}(E) \; p_c(\phi_c) \prod_{i=1}^{L} \left[p_{\phi_{sc_i}}(\phi_{sc_i}) p_{\phi_{sy_i}}(\phi_{sy_i}) \right] \prod_{n=2}^{L} \left[p_{\Delta\phi_{n1}}(\Delta\phi_{n1}) \right] \; d\Delta\phi d\phi_{sc} d\phi_{sy} d\phi_c \tag{55}$$

where the three $\int_{-\infty}^{\infty}$ are with respect to $\phi_{sc} = (\phi_{sc_1}, ..., \phi_{sc_L})$, $\phi_{sy} = (\phi_{sy_1}, ..., \phi_{sy_L})$, and $\Delta\phi = (\Delta\phi_{21}, ..., \Delta\phi_{(L-1)1})$. The conditional SER, denoted P'_{csc}, is given as

$$P'_{csc} = \frac{1}{4}\,\mathrm{erfc}\left[\sqrt{\frac{E_{s1}}{N_{01}}\frac{\left(\sum\limits_{n=1}^{L}\gamma_n^2 C_{sc_n}^2\left(1-\frac{|\phi_{sy_n}|}{\pi}\right)^2 + \sum\limits_{n=1}^{L}\sum\limits_{\substack{m=1\\n\neq m}}^{L}\gamma_n\gamma_m C_{sc_n}C_{sc_m}\left(1-\frac{|\phi_{sy_n}|}{\pi}\right)\left(1-\frac{|\phi_{sy_m}|}{\pi}\right)C_{nm}\right)}{\sum\limits_{n=1}^{L}\gamma_n}}\,C_c\right]$$

$$+ \frac{1}{4}\,\mathrm{erfc}\left[\sqrt{\frac{E_{s1}}{N_{01}}\frac{\left(\sum\limits_{n=1}^{L}\gamma_n^2 C_{sc_n}^2 + \sum\limits_{n=1}^{L}\sum\limits_{\substack{m=1\\n\neq m}}^{L}\gamma_n\gamma_m C_{sc_n}C_{sc_m}C_{nm}\right)}{\sum\limits_{n=1}^{L}\gamma_n}}\,C_c\right] \tag{56}$$

Ideally, when there are no losses, $C_c = C_{sc_n} = (1 - |\phi_{sy_n}|/\pi) = C_{nm} = 1$ and Eq. (55) reduce to $P(E)_{csc} = (1/2)\,\mathrm{erfc}\,(\sqrt{E_s L/N_0})$, for an array of L antennas of the same size (i.e., when $\gamma_n = 1$ for all n). The loss for CSC is given by Eq. (23) with $P_s(E)$ now replaced by Eq. (55).

V. Numerical Results and Discussion

The discussion section is divided into two parts. The first part compares FSC and CSC for an array of two 70-m antennas when the symbol SNR at each antenna is very low (−11 dB) and very high (6 dB). The quantitative results obtained in Section I confirm that degradation and loss are equal at low SNR values, but show that degradation is a lower bound for loss at high symbol SNR values. The second part focuses on the Galileo S-band mission scenario, where the received SNR is expected to be very low. For this part, the FSC and CSC techniques are compared for several different antenna combinations with different symbol rates, using degradation as the performance measure.

A. Degradation Versus Loss

The FSC and CSC performance for an array of two 70-m antennas when the received signal is weak is shown in Fig. 5; results for a strong signal case are shown in Fig. 6(a) for $B_c = 70$ Hz and Fig. 6(b) for $B_c = 160$ Hz. The carrier bandwidth for the strong signal case was widened from 70 to 160 Hz to demonstrate the difference between degradation and loss as the carrier loop SNR becomes low. Inspection of these figures shows that degradation and loss are equal (within 0.01 dB) for weak signal levels, but degradation is a lower bound for loss at strong signal levels.

Consequently, the generally relative performance measure of degradation can be used at low symbol SNR's to make an absolute assessment of the received system. It is shown later that the advantange of being able to use degradation instead of loss at low symbol SNR's is a significant savings in computation time. Clearly, if all harmonics of the subcarrier are used (see Section V-B), FSC outperforms CSC except at narrow $W_{sc}B_{sc} = W_{sy}B_{sy}$ where both curves converge.

The weak and strong signals are characterized as follows: weak signal is $P_1/N_{01} = P_2/N_{02} = 15$ dB-Hz, $R_{sym} = 1/T = 400$ sym/sec; strong signal is $P_1/N_{01} = P_2/N_{02} = 32$ dB-Hz, $R_{sym} = 1/T = 400$ sym/sec. Note that the weak signal's uncombined SNR $E_{s1}/N_{01} = E_{s2}N_{01} = -11$ dB, whereas the strong signal's $E_{s1}/N_{01} = E_{s2}/N_{01} = 6$ dB. For an ideal system, there is a 3-dB arraying gain so that the combined E_s/N_0 for the weak signal case is −8 dB, which corresponds[6] to an SER = 0.286942, and the combined E_s/N_0 in the strong signal case is 9 dB, for which the SER = 3.4 × 10^{-5}. The receiver parameters for FSC and CSC in the weak signal case are assumed to be as follows: $B_c = 0.1$ Hz, B_{sc} and B_{sy} are variable, $B_{corr} = 4$ kHz (FSC only), and $T_c = 120$ sec. The following parameters apply to the strong signal case: $B_c = 70$ Hz and $B_c = 160$ Hz, B_{sc} and B_{sy} are variable, $B_{corr} = 4$ kHz (FSC only), and $T_c = 120$ sec. Furthermore, the FSC correlator is assumed to operate only on fundamental subcarrier harmonics, i.e., $L_{sc} = 1$ in Eq. (31).

The degradation in these figures is found through Eq. (34) for FSC and Eq. (54) for CSC. The loss curves

---

[6] $P(E)_{ideal} = \frac{1}{2}\mathrm{erfc}\left(\sqrt{(E_s/N_0)L}\right)$ for L antennas of the same size.

are computed using Eqs. (23) and (35) for FSC and Eqs. (23) and (55) for CSC. The loss computation is an iterative process that uses a trial-and-error method as shown by the following example. Suppose the FSC loss for $W_{sc}B_{sc} = W_{sy}B_{sy} = 2$ mHz in Fig. 5 is to be computed. First, the FSC SER is computed[7] through Eq. (35) with $E_s/N_0 = -11$ dB. The resulting SER is 0.2916693, which is higher that the ideal SER of 0.286942. Consequently, a second computation of Eq. (35) is made with $E_s/N_0 = -11$ dB $+ \Delta E_s/N_0$. If the resulting SER is 0.286942, then the loss is said to be $\Delta E_s/N_0$. If the resulting SER is greater or less than 0.286942, then Eq. (35) is recomputed with different $\Delta E_s/N_0$ values until the SER is equal to the ideal SER. The value of $\Delta E_s/N_0$, which results in Eq. (35) equaling the ideal SNR, is by definition the loss. For this example, $\Delta E_s/N_0$ or the symbol SNR loss was found to be 0.2 dB. This method is clearly more difficult than degradation, which is a single computation devoid of integrals. Nevertheless, symbol SNR loss gives the absolute performance advantage of an arraying scheme, while symbol SNR degradation gives the relative performance advantage. The loop and correlator SNR's used in obtaining Figs. 5 and 6 are shown in Tables 3 and 4. The FSC loop SNR's are computed from Eqs. (9)–(11) using the average combined power found by averaging Eq. (26) over the residual phase and dividing by the effective noise level in Eq. (24). The CSC subcarrier and symbol loop SNR's are computed using Eqs. (39) and (40), respectively. However, the carrier loop SNR for CSC uses the average combined power $P'/N_{0_{eff}}$, which is found by averaging Eq. (47) over all the phases and then dividing by the effective noise level. Moreover, the correlation SNR's for FSC and CSC were computed using Eqs. (31) and (51), respectively.

B. Galileo S-Band Mission Scenario

The FSC and CSC performance for different combinations of 70-m and 34-m antennas is discussed in this section. Since Galileo has a weak signal, the performance measure used is degradation, although loss could have also been used, as demonstrated in Fig. 5. As pointed out in the introduction, the IF signals in FSC are typically transmitted to a central location before being combined and demodulated using a single receiver. However, since the retransmission channel is band-limited, signal energy may be lost prior to combining. Table 5 shows energy lost as a function of the number of subcarrier harmonics present at the central location (i.e., at the combiner input). For the Galileo scenerio, four subcarrier harmonics are present at

the combiner input, and the energy lost is 0.22 dB. The retransmission of CSC signals to a central location, on the other hand, does not result in an energy loss because the symbol rates for Galileo (less than 640 sym/sec) can be easily supported by the retransmission channel.

1. Array of Two 70-m Antennas. With that background, consider first an array of two 70-m antennas when the signal characteristics and receiver parameters are the same as those in Fig. 5 with $R_{sym} = 400$ sym/sec. FSC performance for the Galileo scenerio is obtained by adding 0.22 dB to the FSC degradation in Fig. 5. The shifted FSC curve along with the CSC degradation (which is the same as in Fig. 5 since no energy is lost in CSC) is plotted in Fig. 7. Notice that both techniques have equal performance when $W_{sc}B_{sc} = W_{sy}B_{sy} = 1.2$ mHz. In addition, Fig. 7 shows results using the same parameters as in Fig. 5, but now with $R_{sym} = 200$ sym/sec (combined $E_s/N_0 = -5.0$ dB). In this case, FSC and CSC have equal performance when $W_{sc}B_{sc} = W_{sy}B_{sy} = 3.0$ mHz. The degradation due to individual components (carrier, subcarrier, symbol, and correlator) is discussed below, indicating the relative contribution of each to the total degradation shown in Fig. 7 for $R_{sym} = 400$ sym/sec.

The degradation due to a single component is defined as the degradation that would be observed when all but a single component are operating ideally. For example, in FSC the degradation due to the carrier loop is given as

$$D_{fsc}\big|_{[SNR_{n1,fsc}=\rho_{sc}=\rho_{sy}=\infty]} = -10 \, \log_{10} \overline{C_c^2} \qquad (57)$$

which is derived by setting the correlation SNR, the subcarrier loop SNR, and the symbol loop SNR to infinity in Eq. (34). The degradation due to individual components is shown in Figs. 8(a), (b), (c), and (d). Table 6 lists the degradation breakdown for FSC and CSC at $W_{sc}B_{sc} = W_{sy}B_{sy} = 5$ mHz and $R_{sym} = 400$ sym/sec. It is evident that the combiner degradation for both schemes is negligible. Also, the carrier degradation is the same for FSC and CSC since the carrier loop SNR for both schemes is about the same. The subcarrier and symbol degradation, however, are significantly different for FSC and CSC, with CSC being greater because the carrier is not tracked nor the signal combined until after the subcarrier and symbol loops. Comparing the sum in Table 6 to Fig. 7 for $R_{sym} = 400$ sym/sec indicates that total degradation can be approximated as the sum of individual degradations.

2. Array of a 70-m and One 34-m STD Antenna. The performance of a 70-m with one 34-m STD

---

[7] Note that the SER in Eqs. (35) and (55) requires numerical integration. An approximation to SER can be derived, however, using the moments techniques described in [10].

antenna array is shown in Fig. 9(a) using the same parameters as in Fig. 5 except $P_1/N_{01} = 15$ dB-Hz and $P_2/N_{02} = 7.3$ dB-Hz, i.e., $\gamma_1 = 1$ and $\gamma_2 = 0.17$ as shown in Table 2. Figure 9(a) also shows the results when $R_{sym} = 200$ sym/sec. At these signal levels, the 34-m antenna is not expected to achieve subcarrier and symbol lock without being aided by the 70-m antenna. Consequently, the CSC arraying scheme is implemented by passing frequency and phase information from the 70-m to the 34-m antenna. As a result, the effective subcarrier and symbol loop SNR's of the 34-m are identical to that of the 70-m antenna. The modified CSC is called CSCA or complex-symbol combining with aiding. In this scenario, the practical FSC outperforms CSCA when $W_{sc}B_{sc} = W_{sy}B_{sy}$ is greater than 4.5 mHz at $R_{sym} = 400$ sym/sec and 10 mHz at $R_{sym} = 200$ sym/sec.

3. Array of a 70-m and Two 34-m STD Antennas. The result for an array of one 70-m and two 34-m antennas is shown in Fig. 9(b). Practical FSC, in this case, outperforms CSCA when $W_{sc}B_{sc} = W_{sy}B_{sy}$ is greater than 4.0 mHz at $R_{sym} = 400$ sym/sec and 8.5 mHz at $R_{sym} = 200$ sym/sec.

4. Array of a 70-m and Three 34-m STD Antennas. For an array of one 70-m and three 34-m antennas, practical FSC outperforms CSCA when $W_{sc}B_{sc} = W_{sy}B_{sy}$ is greater than 3.5 mHz at $R_{sym} = 400$ sym/sec and 8.2 mHz at $R_{sym} = 200$ sym/sec. See Fig. 9(c).

5. Array of Four 34-m STD Antennas. Figure 9(d) shows the result for an array of four 34-m antennas for $R_{sym} = 50$ sym/sec and $R_{sym} = 25$ sym/sec with

$B_{corr} = 400$ Hz. For this array, FSC has less degradation than CSC when $W_{sc}B_{sc} = W_{sy}B_{sy}$ are above 0.32 mHz when $R_{sym} = 50$ sym/sec and above 0.8 mHz when $R_{sym} = 25$ sym/sec. Practical FSC is able to operate for the given $W_{sc}B_{sc} = W_{sy}B_{sy}$ without losing lock, assuming the subcarrier and symbol loops are able to lock to the signal if their respective loop SNR's are greater than 12 dB. For CSC, however, the maximum $W_{sc}B_{sc} = W_{sy}B_{sy}$ that can be supported without losing lock is about 0.9 mHz[8] at $R_{sym} = 50$ sym/sec and 2 mHz at $R_{sym} = 25$ sym/sec. Table 7 lists the break-even points for the different combinations of a 70-m and 34-m antennas mentioned.

VI. Conclusion

This article describes the performance of FSC and CSC in terms of symbol SNR degradation and symbol SNR loss. Both degradation and loss are approximately equal at low values of symbol SNR, but diverge at high SNR values. For arrays of two 70-m antennas, a 70-m and three 34-m antennas, a 70-m and two 34-m antennas, and a 70-m and one 34-m antenna, FSC has less degradation than CSC when $W_{sc}B_{sc} = W_{sy}B_{sy}$ are above 3.0, 10.0, 8.5, and 8.2 mHz at $R_{sym} = 200$ sym/sec, and 1.2, 4.5, 4.0, and 3.5 mHz at $R_{sym} = 400$ sym/sec, respectively. Moreover, for an array of four 34-m antennas, FSC has less degradation than CSC when $W_{sc}B_{sc} = W_{sy}B_{sy}$ are above 0.32 mHz at $R_{sym} = 50$ sym/sec and above 0.8 mHz at $R_{sym} = 25$ sym/sec.

---

[8] This point can be increased by using the average of the four phase estimates of the subcarrier and symbol loops to effectively improve the loop SNR by about 6 dB, so that the degradation is lessened.

Acknowledgments

References

[1] A. Mileant and S. Hinedi, "Overview of Arraying Techniques for Deep Space Communications," to be published in *IEEE Trans. Commun.*

[2] S. Hinedi, "NASA's Next Generation All-Digital Deep Space Network Breadboard Receiver," *IEEE Trans. on Commun.*, vol. 41, pp. 246–257, January 1993.

[3] D. Divsalar, "Symbol Stream Combining Versus Baseband Combining for Telemetry Arraying," *The Telecommunications and Data Acquisition Progress Report 42-74, vol. April–June 1983*, Jet Propulsion Laboratory, Pasadena, California, pp. 13–28, August 15, 1983.

[4] M. Shihabi, T. Nguyen, and S. Hinedi, "On the Use of Subcarrier in Future Space Missions," *IEEE Trans. on EMC*, February 1994.

[5] W. J. Hurd and S. Aguirre, "A Method to Dramatically Improve Subcarrier Tracking," *IEEE Trans. on Commun.*, vol. 36, pp. 238–243, February 1988.

[6] M. K. Simon, "Analysis of the Steady State Phase Noise Performance of a Digital Data-Transition Tracking Loop," *Space Programs Summary 37-55*, vol. 3, Jet Propulsion Laboratory, Pasadena, California, pp. 54–62, February 1969.

[7] R. Sfeir, S. Aguirre, and W. J. Hurd, "Coherent Digital Demodulation of a Residual Carrier Signal Using IF Sampling," *The Telecommunications and Data Acquisition Progress Report 42-78, vol. April–June 1984*, Jet Propulsion Laboratory, Pasadena, California, pp. 135–142, August 15, 1984.

[8] J. H. Yuen, *Deep Space Telecommunications Systems Engineering*, New York: Plenum Press, 1983.

[9] W. C. Lindsey and M. K. Simon, *Telecommunication Systems Engineering*, New Jersey: Prentice-Hall, Inc., 1973.

[10] J. K. Omura and M. K. Simon, *Satellite Communication Performance Evaluation: Computational Techniques Based on Moments*, JPL Publication 80-71, Jet Propulsion Laboratory, Pasadena, California, September 15, 1980.

Table 1. Comparison of FSC and CSC.

Parameter	FSC	CSC
Combining bandwidth	Sample rate	Sample rate
Carrier loop	Closed before subcarrier and symbol loops	Closed after subcarrier and symbol loops
Effective P/N_0 at input of subcarrier loop for two 70-m antennas		At least 6 dB lower than FSC when carrier is unlocked and 3 dB lower when carrier locked
Effective P/N_0 at input of symbol loop for two 70-m antennas		At least 6 dB lower than FSC when carrier is unlocked and 3 dB lower when carrier locked
Array of a 70- and 34-m antenna	Loops operate on the combined signal power	Phase and frequency information passed from 70- to 34-m antenna
Array of four 34-m antennas	Implementable	Harder to implement

Table 2. Gamma factors for DSN antennas.

Antenna size	Frequency band	γ_n
70 m	S-band	1.00
34 m STD	S-band	0.17
34 m HEF	S-band	0.07
70 m	X-band	1.00
34 m STD	X-band	0.13
34 m HEF	X-band	0.26

Table 3(a). FSC loop SNR's for SER = 0.286942.

$W_{sc}B_{sc} = W_{sy}B_{sy}$, mHz	Carrier loop SNR, dB	Subcarrier loop SNR, dB	Symbol loop SNR, dB	Correlator SNR, dB
0.01	21.8	57.9	46.0	15.9
0.1	21.8	47.9	36.0	15.9
0.3	21.8	43.1	31.3	15.9
0.5	21.8	40.9	29.0	15.9
0.7	21.8	39.4	27.6	15.9
0.9	21.8	38.3	26.5	15.9
2.0	21.8	34.9	23.0	15.9
4.0	21.8	31.8	20.0	15.9
6.0	21.8	30.1	18.2	15.9
8.0	21.8	28.8	17.0	15.9
10.0	21.8	27.9	16.0	15.9

Table 3(b). CSC loop SNR's for SER = 0.286942.

$W_{sc}B_{sc} = W_{sy}B_{sy}$, mHz	Carrier loop SNR, dB	Subcarrier loop SNR, dB	Symbol loop SNR, dB	Correlator SNR, dB
0.01	21.8	49.7	37.2	24.1
0.1	21.6	39.7	27.2	24.0
0.3	21.5	35.0	22.5	23.8
0.5	21.4	32.7	20.2	23.7
0.7	21.4	31.3	18.8	23.7
0.9	21.3	30.2	17.7	23.6
2.0	21.1	26.7	14.2	23.3
4.0	20.8	23.7	11.2	23.0
6.0	20.5	21.9	9.4	22.7
8.0	20.3	20.7	8.2	22.5
10.0	20.1	19.7	7.2	22.3

Table 4(a). FSC loop SNR's for SER = 3.4 × 10^{-5}.

$W_{sc}B_{sc} = W_{sy}B_{sy}$, mHz	Carrier loop SNR, dB		Subcarrier loop SNR, dB	Symbol loop SNR, dB	Correlator SNR, dB
	$B_c = 160$ Hz	$B_c = 70$ Hz			
0.01	12.7	16.3	80.8	72.1	47.8
0.1	12.7	16.3	70.8	62.1	47.8
1.0	12.7	16.3	60.8	52.1	47.8
10.0	12.7	16.3	50.8	42.1	47.8
100.0	12.7	16.3	40.8	32.1	47.8
1000.0	12.7	16.3	30.8	22.1	47.8

Table 4(b). CSC loop SNR's for SER = 3.4 × 10^{-5}.

$W_{sc}B_{sc} = W_{sy}B_{sy}$, mHz	Carrier loop SNR, dB		Subcarrier loop SNR, dB	Symbol loop SNR, dB	Correlator SNR, dB
	$B_c = 160$ Hz	$B_c = 70$ Hz			
0.01	12.7	16.3	77.1	67.3	49.3
0.1	12.7	16.3	67.1	57.3	49.3
1.0	12.7	16.3	57.1	47.3	49.3
10.0	12.7	16.3	47.1	37.3	49.2
100.0	12.6	16.2	37.1	27.3	49.1
1000.0	12.3	15.9	27.1	17.3	48.7

Table 5. Number of subcarrier harmonics versus loss in energy.

Number of subcarrier harmonics	Loss in energy, dB
1	0.91
2	0.45
3	0.30
4	0.22
5	0.18
6	0.15
7	0.13
8	0.11
9	0.10
10	0.07

Table 6. Degradation breakdown for two 70-m antennas at $W_{sc}\,B_{sc} = W_{sy}\,B_{sy} = 5$ mHz.

Degradation	FSC, dB	CSC, dB
Combiner	0.034	0.002
Carrier loop	0.029 $\rho_c = 21.8$	0.038 $\rho_c = 20.6$
Subcarrier loop	0.126 $\rho_{sc} = 30.8$	0.324 $\rho_{sc} = 22.7$
Symbol loop	0.124 $\rho_{sy} = 19.0$	0.342 $\rho_{sy} = 10.2$
Energy loss	0.22	0
Sum	0.533	0.708

Table 7. Break-even point for FSC and CSC.

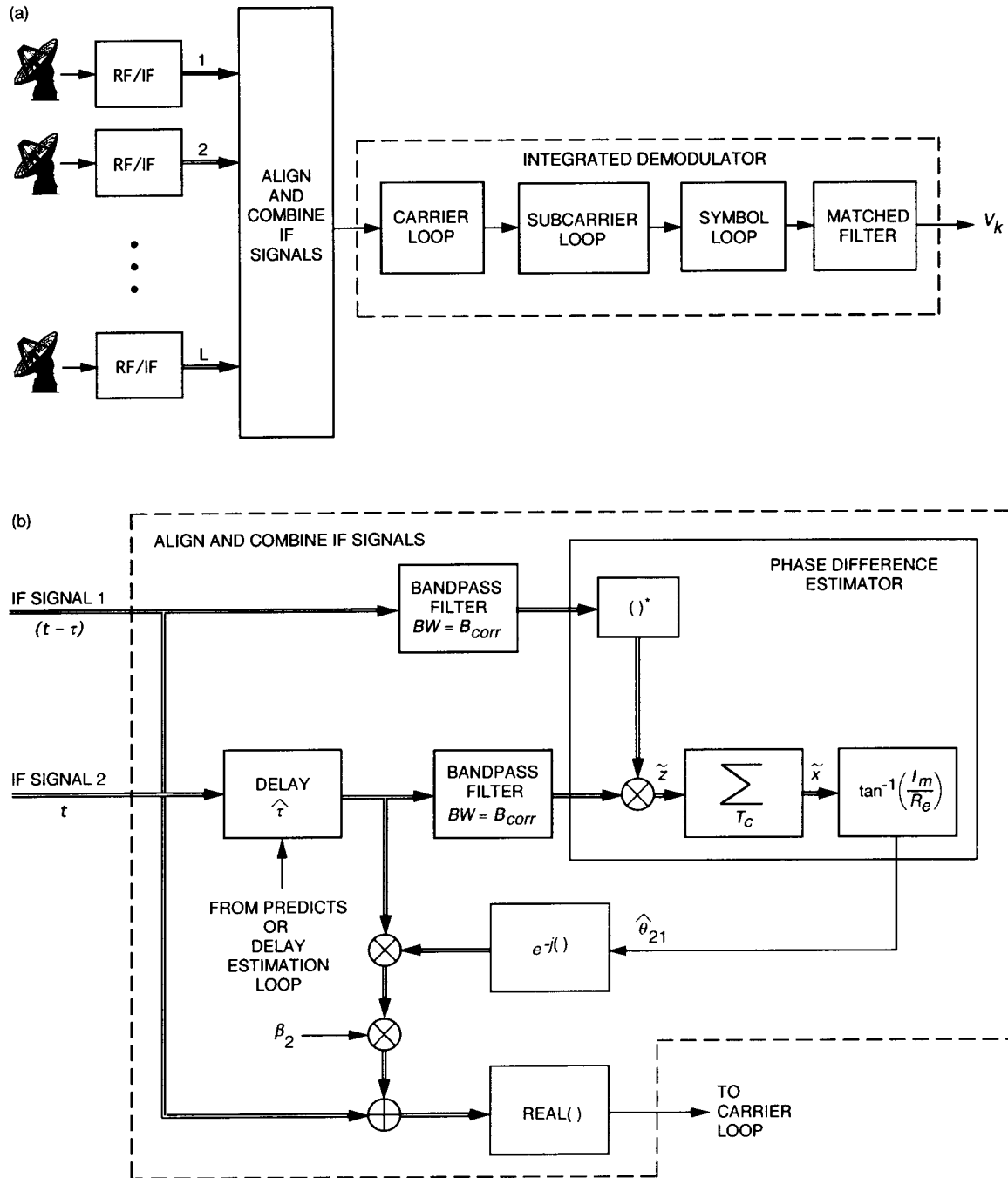| Antenna array	Value of $W_{sy}B_{sy} = W_{sc}B_{sc}$ (mHz) where $D_{fsc} = D_{csc}$		Value of $W_{sy}B_{sy} = W_{sc}B_{sc}$ (mHz) where $D_{fsc} > D_{csc}$		Value of $W_{sy}B_{sy} = W_{sc}B_{sc}$ (mHz) where $D_{fsc} > D_{csc}$	
	$R_{sym} = 200$ Hz	$R_{sym} = 400$ Hz	$R_{sym} = 200$ Hz	$R_{sym} = 400$ Hz	$R_{sym} = 200$ Hz	$R_{sym} = 400$ Hz
Two 70-m	3.0	1.2	>3.0	>1.2	<3.0	<1.2
70- and three 34-m	8.2	3.5	>8.2	>3.5	<8.2	<3.5
70- and two 34-m	8.5	4.0	>8.5	>4.0	<8.5	<4.0
70- and one 34-m	10.0	4.5	>10.0	>4.5	<10.0	<4.4

Fig. 1. Full-spectrum combining (FSC) algorithm: (a) L antenna array and (b) align-and-combine for an array of two antennas.
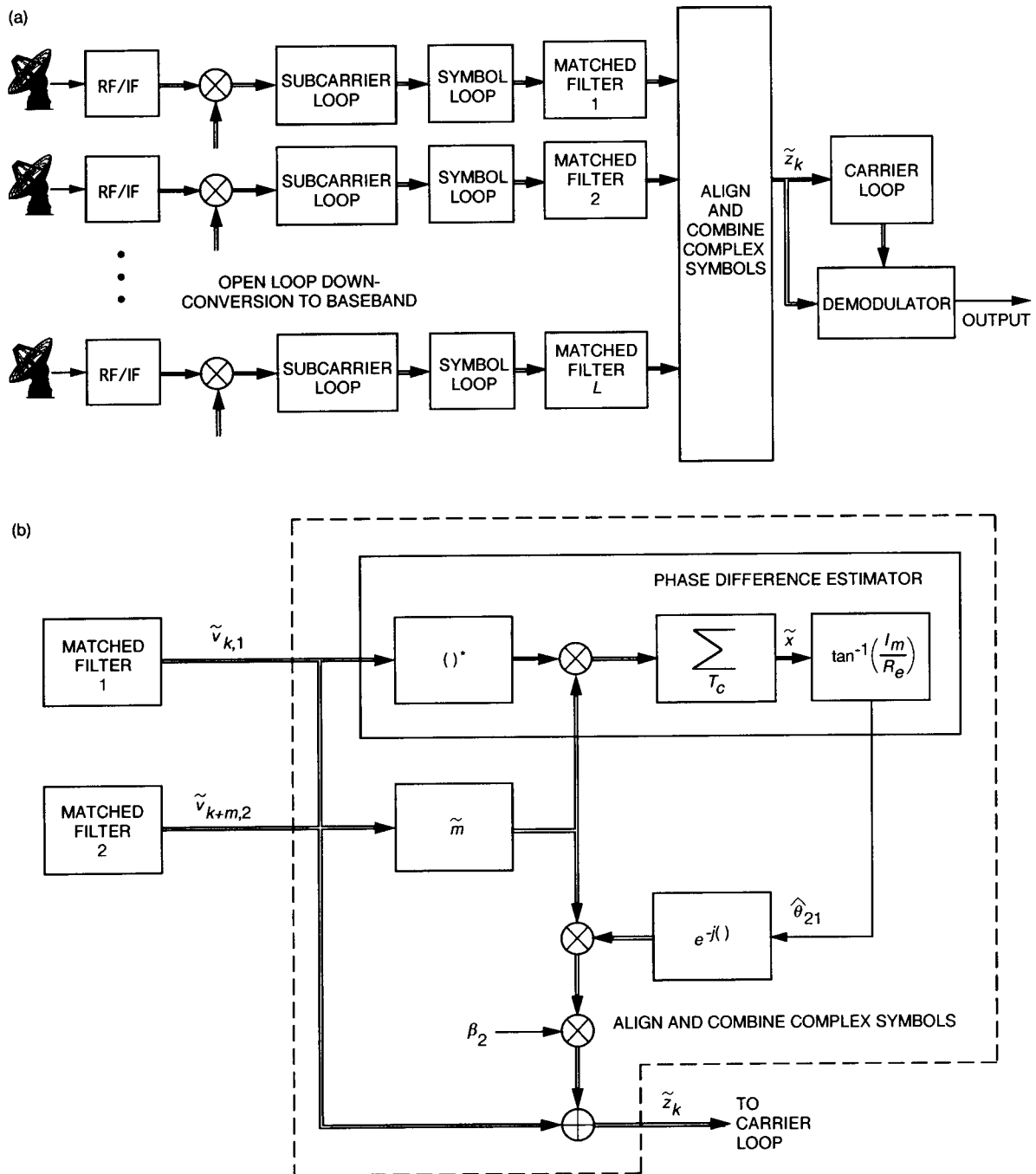
Fig. 2. Complex-symbol combining (CSC) algorithm: (a) L antenna array and (b) align-and-combine for an array of two antennas.
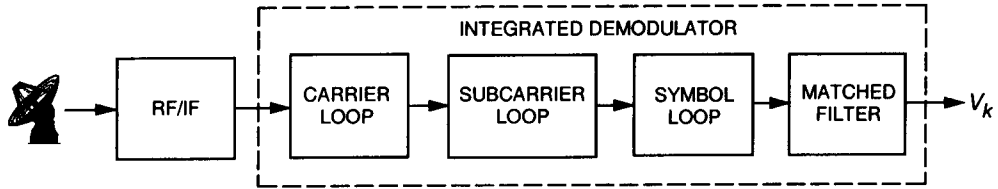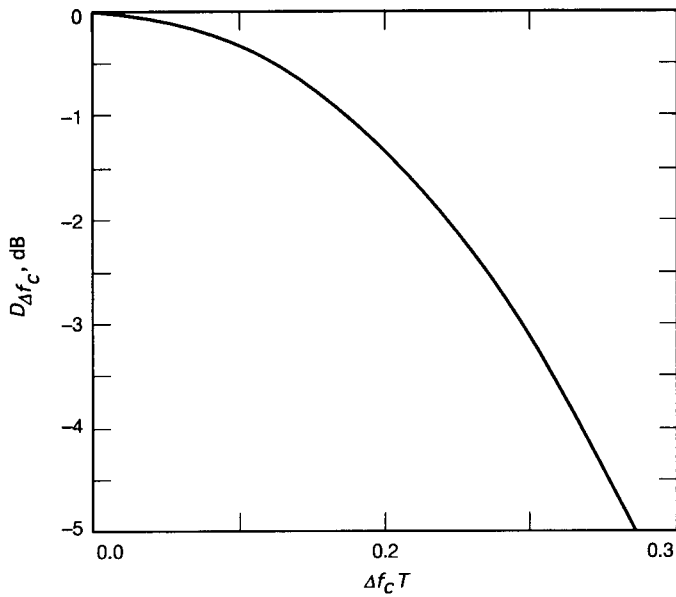
Fig. 3. A general coherent receiver model.

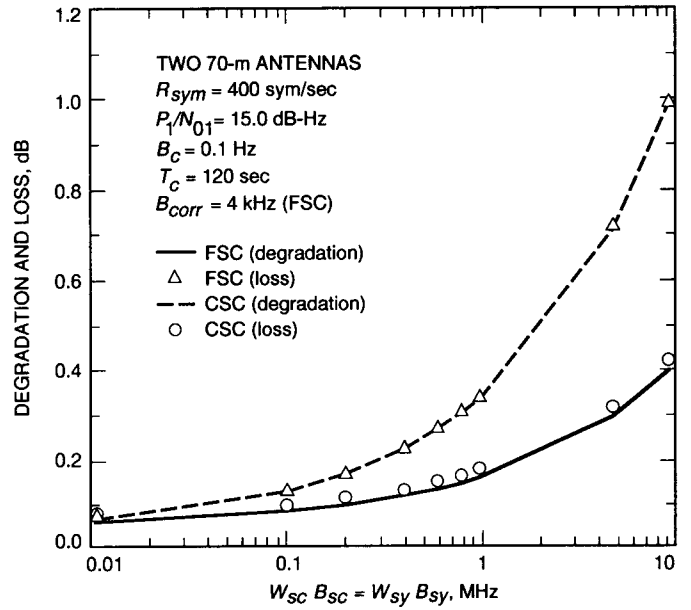Fig. 4. Degradation at the matched filter output versus carrier frequency error-symbol time product.

Fig. 5. Degradation and loss versus subcarrier and symbol window-loop bandwidth for SER = 0.286942.
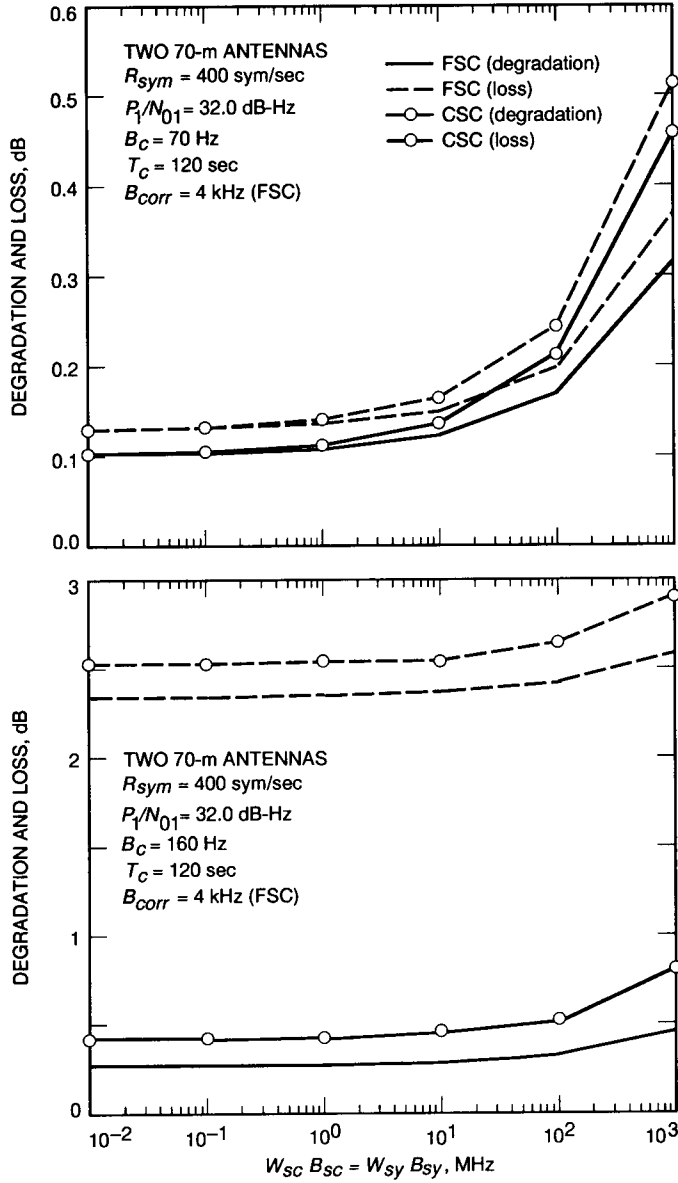
Fig. 6 (top plot):

TWO 70-m ANTENNAS
R_{sym} = 400 sym/sec
P_1/N_{01} = 32.0 dB-Hz
B_C = 70 Hz
T_C = 120 sec
B_{corr} = 4 kHz (FSC)

—— FSC (degradation)
- - - FSC (loss)
—O— CSC (degradation)
—O— CSC (loss)

DEGRADATION AND LOSS, dB

0.6 0.5 0.4 0.3 0.2 0.1 0.0

Fig. 6 (bottom plot):

TWO 70-m ANTENNAS
R_{sym} = 400 sym/sec
P_1/N_{01} = 32.0 dB-Hz
B_C = 160 Hz
T_C = 120 sec
B_{corr} = 4 kHz (FSC)

DEGRADATION AND LOSS, dB

3 2 1 0

$W_{sc} B_{sc} = W_{sy} B_{sy}$, MHz

10^{-2} 10^{-1} 10^0 10^1 10^2 10^3

Fig. 6. A comparison of degradation and loss versus subcarrier
and symbol window-loop bandwidth: (a) SER = 3.4 × 10^{-5} at
Bc = 70 Hz and (b) SER = 3.4 × 10^{-5} at Bc = 160 Hz.

Fig. 7:

TWO 70-m ANTENNAS
P_1/N_{01} = 15.0 dB-Hz
B_C = 0.1 Hz
T_C = 120 sec
B_{corr} = 4 kHz (FSC)

—— FSC, R_{sym} = 200 sym/sec
- - - CSCA, R_{sym} = 200 sym/sec
—O— FSC, R_{sym} = 400 sym/sec
—O— CSCA, R_{sym} = 400 sym/sec

DEGRADATION AND LOSS, dB

1.2 1.0 0.8 0.6 0.4 0.2 0.0

$W_{sc} B_{sc} = W_{sy} B_{sy}$, MHz
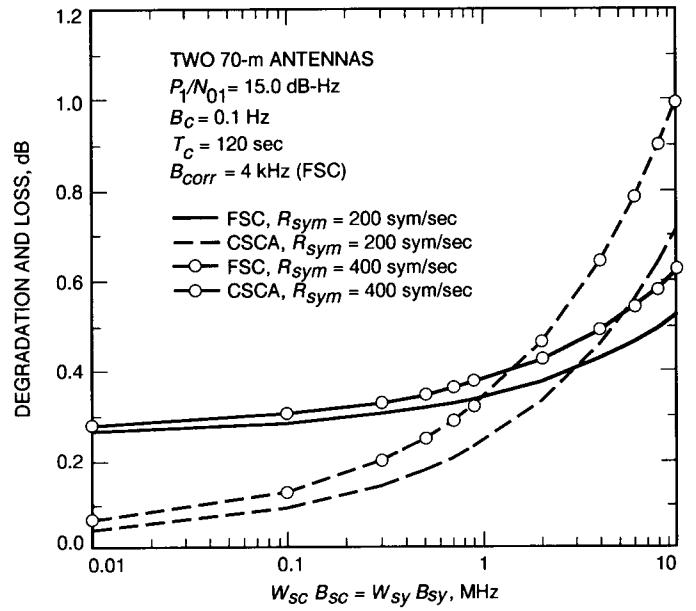
0.01 0.1 1 10

Fig. 7. Practical FSC and CSC degradation versus subcarrier and
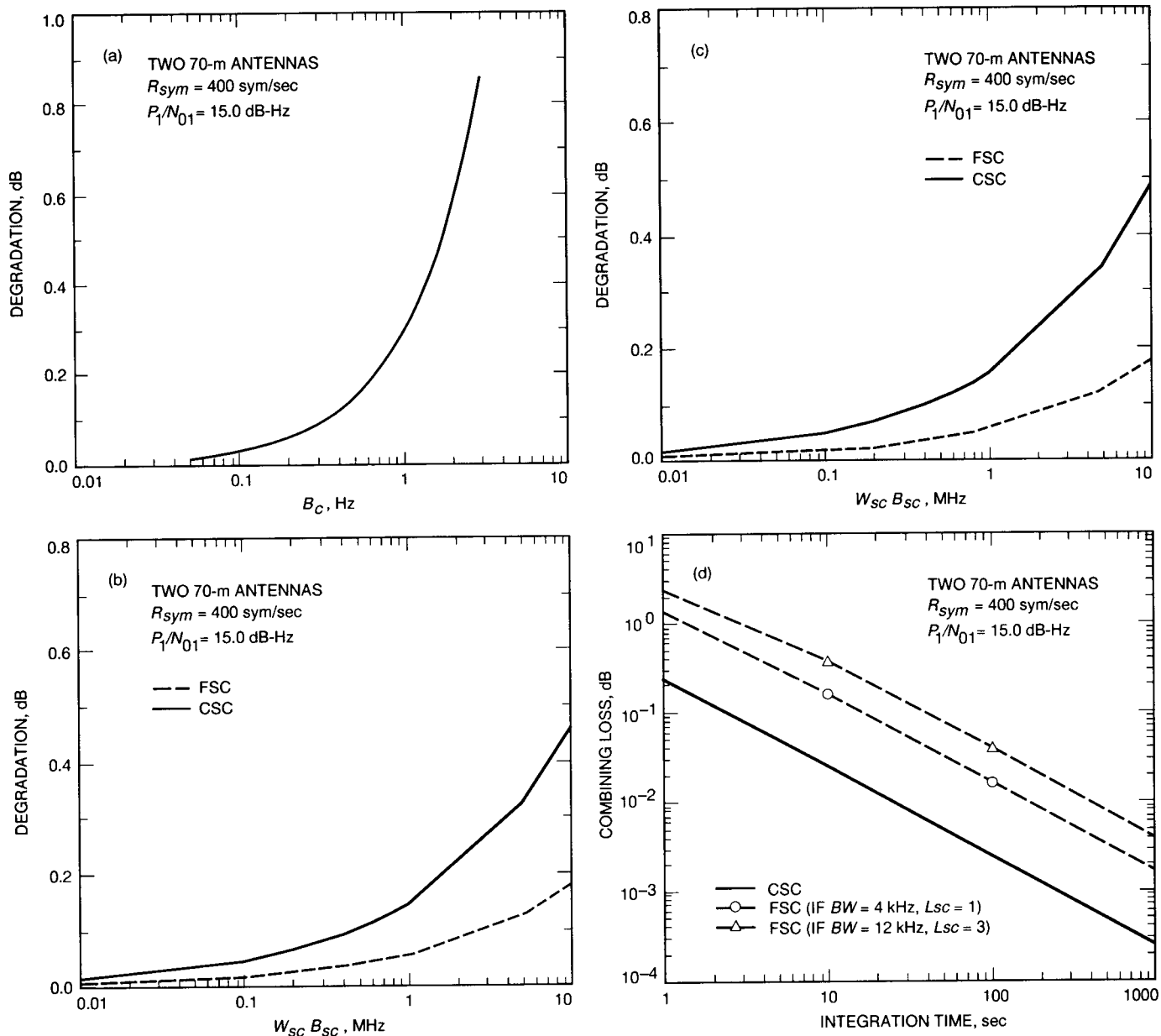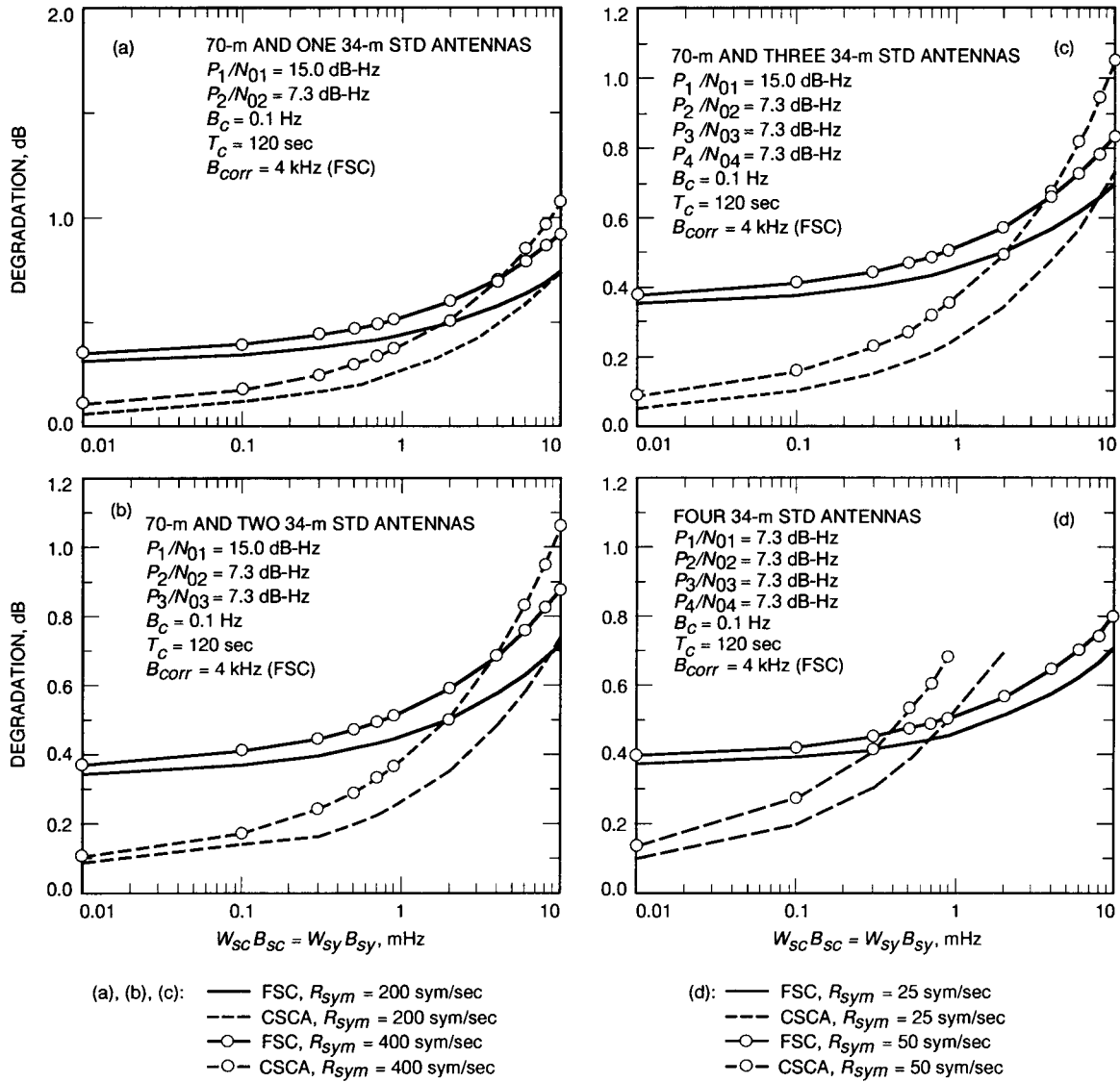symbol window-loop bandwidth.

Fig. 8. Comparisons of degradation due to individual components: (a) carrier degradation versus carrier bandwidth; (b) subcarrier degradation versus subcarrier window-loop bandwidth; (c) symbol degradation versus symbol window-loop bandwidth; and (d) combining loss versus integration time.

(a) 70-m AND ONE 34-m STD ANTENNAS
$P_1/N_{01} = 15.0$ dB-Hz
$P_2/N_{02} = 7.3$ dB-Hz
$B_C = 0.1$ Hz
$T_C = 120$ sec
$B_{corr} = 4$ kHz (FSC)

(c) 70-m AND THREE 34-m STD ANTENNAS
$P_1/N_{01} = 15.0$ dB-Hz
$P_2/N_{02} = 7.3$ dB-Hz
$P_3/N_{03} = 7.3$ dB-Hz
$P_4/N_{04} = 7.3$ dB-Hz
$B_C = 0.1$ Hz
$T_C = 120$ sec
$B_{corr} = 4$ kHz (FSC)

(b) 70-m AND TWO 34-m STD ANTENNAS
$P_1/N_{01} = 15.0$ dB-Hz
$P_2/N_{02} = 7.3$ dB-Hz
$P_3/N_{03} = 7.3$ dB-Hz
$B_C = 0.1$ Hz
$T_C = 120$ sec
$B_{corr} = 4$ kHz (FSC)

(d) FOUR 34-m STD ANTENNAS
$P_1/N_{01} = 7.3$ dB-Hz
$P_2/N_{02} = 7.3$ dB-Hz
$P_3/N_{03} = 7.3$ dB-Hz
$P_4/N_{04} = 7.3$ dB-Hz
$B_C = 0.1$ Hz
$T_C = 120$ sec
$B_{corr} = 4$ kHz (FSC)

DEGRADATION, dB

$W_{sc}B_{sc} = W_{sy}B_{sy}$, mHz

(a), (b), (c):
——— FSC, $R_{sym} = 200$ sym/sec
- - - CSCA, $R_{sym} = 200$ sym/sec
–O– FSC, $R_{sym} = 400$ sym/sec
–O– CSCA, $R_{sym} = 400$ sym/sec

(d):
——— FSC, $R_{sym} = 25$ sym/sec
- - - CSCA, $R_{sym} = 25$ sym/sec
–O– FSC, $R_{sym} = 50$ sym/sec
–O– CSCA, $R_{sym} = 50$ sym/sec

Fig. 9. Comparisons of degradation for various array configurations: (a) one 70-m and one 34-m STD antennas; (b) one 70-m and two 34-m STD antennas; (c) one 70-m and three 34-m STD antennas; and (d) four 34-m STD antennas.

Appendix A

The Performance of the FSC Correlator

The performance of the FSC correlator is derived here for the general case when total power is divided between data as well as the carrier. Once the general correlator SNR is derived, it will be simplified for the Galileo case, which operates with the carrier fully suppressed. As shown in Fig. 1(b), combining at IF requires both delay and phase adjustments in order to coherently add the signals. Here, perfect knowledge of the time delay is assumed and only phase compensation is needed before adding the IF signals. The IF signal at antenna n, denoted by the double lines in Fig. 1(b), consists of an in-phase (I) and quadrature (Q) component given as $r_{nI}(t)$ and $r_{nQ}(t)$, respectively, as follows:

$$r_{nI}(t) = \sqrt{2P_c}\cos(\omega_c t + \theta_{cn}) - \sqrt{2P_d}d(t)\mathrm{Sqr}(\omega_{sc}t + \theta_{sc_n})\sin(\omega_c t + \theta_{cn}) + n_{nI}(t) \tag{A-1}$$

$$r_{nQ}(t) = \sqrt{2P_c}\sin(\omega_c t + \theta_{cn}) + \sqrt{2P_d}d(t)\mathrm{Sqr}(\omega_{sc}t + \theta_{sc_n})\cos(\omega_c t + \theta_{cn}) + n_{nQ}(t) \tag{A-2}$$

where the total power P in watts (W) is divided between the residual carrier and data by controlling the modulation index, Δ. Specifically, the carrier power $P_c = P\cos^2\Delta$ and the data power[1] $P_d = P\sin^2\Delta$. Also, $n_{nI}(t)$ and $n_{nQ}(t)$ are statistically independent with a flat one-sided PSD level equal to N_0 W/Hz, and all other relevant parameters are defined in the main text. The square-wave subcarrier defined above can be expressed as follows:

$$\mathrm{Sqr}(\omega_{sc}t + \theta_{sc_n}) = \frac{4}{\pi}\sum_{\substack{j=1\\j:odd}}^{L_{sc}}\frac{\sin[j(\omega_{sc}t + \theta_{sc_n})]}{j} \tag{A-3}$$

where L_{sc}, the number of subcarrier harmonics, is infinite. As shown in Fig. 1(b), the IF signal from antenna 1 and n are first bandpass filtered with single-sided bandwidth B_{corr}, and then complex correlated. The output of the correlation, denoted $\tilde{z}$, is a complex signal consisting of a real (I) and imaginary (Q) component, i.e.,

$$\tilde{z} = I + jQ \tag{A-4}$$

The correlator SNR at $\tilde{z}$, denoted as $SNR'_{n1,fsc}$, is defined as

$$SNR'_{n1,fsc} \triangleq \frac{E(\tilde{z})E(\tilde{z}^*)}{Var(\tilde{z})} = \frac{E(\tilde{z})E(\tilde{z}^*)}{E(\tilde{z}\tilde{z}^*) - E(\tilde{z})E(\tilde{z}^*)}$$

$$= \frac{E^2(I) + E^2(Q)}{Var(I) + Var(Q)} \tag{A-5}$$

where $*$ represents the complex conjugate operation. Following the correlation, an averaging operation over T_c sec is performed to reduce the noise effect. In that period, $N = 2B_{corr}T_c$ independent samples are used to reduce the variance by a factor of N. The SNR at $\tilde{x}$, denoted $SNR_{n1,fsc}$, is thus given by

---

[1] For the Galileo case, $\Delta = 90$ deg so that $P_c = 0$ and $P = P_d$.

$$SNR_{n1,fsc} = SNR'_{n1,fsc}N$$

$$= SNR'_{n1,fsc}(2B_{corr}T_c) \qquad \text{(A-6)}$$

For the general case of any L_{sc}, the correlator SNR using Eq. (A-5) can be shown to be

$$SNR'_{n1,fsc} = \frac{4P_{c1}P_{cn} + 4\left(\dfrac{4}{\pi}\right)^2 \sqrt{P_{c1}P_{cn}P_{d1}P_{dn}}\left[\displaystyle\sum_{\substack{j=1\\jodd}}^{L_{sc}}\left(\dfrac{1}{j}\right)^2\right] + \left(\dfrac{4}{\pi}\right)^4 P_{d1}P_{dn}\left[\displaystyle\sum_{\substack{j=1\\jodd}}^{L_{sc}}\left(\dfrac{1}{j}\right)^2\right]^2}{4N_oB_{corr}\left[P_{c1} + P_{cn} + \dfrac{1}{2}\left(\dfrac{4}{\pi}\right)^2(P_{d1}+P_{dn})\left(\displaystyle\sum_{\substack{j=1\\jodd}}^{L_{sc}}\left(\dfrac{1}{j}\right)^2\right) + B_{corr}\right]} \qquad \text{(A-7)}$$

where B_{corr} is assumed to be sufficiently wide to pass the L_{sc} subcarrier harmonic unfiltered. The correlator SNR at the output of the accumulator is now obtained by using Eq. (A-6) and, after simplification, is given as

$$SNR_{n1} = \frac{T_c\left(2\dfrac{P_{c1}}{N_{01}}\dfrac{P_{cn}}{N_{0n}} + 2\left(\dfrac{4}{\pi}\right)^2\sqrt{\dfrac{P_{c1}}{N_{01}}\dfrac{P_{cn}}{N_{0n}}\dfrac{P_{d1}}{N_{01}}\dfrac{P_{dn}}{N_{0n}}\left(\displaystyle\sum_{\substack{j=1\\jodd}}^{L}\left(\dfrac{1}{j}\right)^2\right) + \dfrac{1}{2}\left(\dfrac{4}{\pi}\right)^4\dfrac{P_{d1}}{N_{01}}\dfrac{P_{dn}}{N_{0n}}\left(\displaystyle\sum_{\substack{j=1\\jodd}}^{L}\left(\dfrac{1}{j}\right)^2\right)^2\right)}{\dfrac{P_{c1}}{N_{01}} + \dfrac{P_{cn}}{N_{0n}} + \dfrac{1}{2}\left(\dfrac{4}{\pi}\right)^2\left(\dfrac{P_{d1}}{N_{01}} + \dfrac{P_{dn}}{N_{0n}}\right)\left(\displaystyle\sum_{\substack{j=1\\jodd}}^{L}\left(\dfrac{1}{j}\right)^2\right) + B_{corr}} \qquad \text{(A-8)}$$

For $\Delta = 90$ deg, Eq. (A-8) is reduced to Eq. (31). In addition, setting $\Delta = 0$ deg in Eq. (A-8) results in the same expression for the correlator SNR as that given in [1].

Appendix B

Subcarrier and Symbol Loop SNR Performance

I. Subcarrier Loop SNR Performance

Compared to the conventional unmodified subcarrier loop, which employs the I-arm as shown in Fig. B-1, the modified subcarrier loop, depicted in Fig. B-2, utilizes both the I and Q arms of the baseband signal for tracking. The loop SNR for both schemes is derived here and compared to the case when the carrier is locked. For CSC, the I and Q channels at the input of the subcarrier loop are respectively given as

$$I(t_n) = \sqrt{P}d(t_n)\text{Sqr}(\omega_{sc}t_n + \theta_{sc})\cos{(\Delta\omega_c t_n)} + n_I(t_n) \tag{B-1}$$

$$Q(t_n) = \sqrt{P}d(t_n)\text{Sqr}(\omega_{sc}t_n + \theta_{sc})\sin{(\Delta\omega_c t_n)} + n_Q(t_n) \tag{B-2}$$

where $n_I(t_n)$ and $n_Q(t_n)$ are independent Gaussian noise processes and all other parameters were previously defined. As shown in Fig. B-2, both the I and Q components are multiplied by the square-wave references and averaged over one symbol period (assuming perfect symbol synchronization), resulting in [5]

$$I_s(k) = \sqrt{P}d_k f(\phi_{sc})\cos{(\Delta\omega_c t_k)} + n_{Is}(k) \tag{B-3}$$

$$I_c(k) = \sqrt{P}d_k g(\phi_{sc})\cos{(\Delta\omega_c t_k)} + n_{Ic}(k) \tag{B-4}$$

$$Q_s(k) = \sqrt{P}d_k f(\phi_{sc})\sin{(\Delta\omega_c t_k)} + n_{Qs}(k) \tag{B-5}$$

$$Q_c(k) = \sqrt{P}d_k g(\phi_{sc})\sin{(\Delta\omega_c t_k)} + n_{Qc}(k) \tag{B-6}$$

where k denotes the symbol index, $f(\phi_{sc}) = 1 - 2/\pi|\phi_{sc}|$ for $|\phi_{sc}| \leq \pi$, $g(\phi_{sc}) = 2/\pi\ \phi_{sc}$ for $|\phi_{sc}| \leq \pi W_{sc}/2$, and $\text{Var}[n_{Is}(k)] = \text{Var}[n_{Ic}(k)] = \text{Var}[n_{Qs}(k)] = \text{Var}[n_{Qc}(k)] = \sigma_n^2 = N_0/2T$. The error signals of the conventional and modified subcarrier loops are respectively given as

$$e(k)_I = Pf(\phi_{sc})g(\phi_{sc})\cos^2(\Delta\omega_c t_k) + N_I(k) \tag{B-7}$$

$$e(k)_{IQ} = Pf(\phi_{sc})g(\phi_{sc}) + N_{IQ}(k) \tag{B-8}$$

where the variance of the noise terms respectively (after averaging over $\Delta\omega_c t_k$, assuming uniform distribution) are given as

$$\sigma_{N_{IQ}}^2 = P\sigma_n^2 + 2\sigma_n^4 \tag{B-9}$$

$$\sigma_{N_I}^2 = \frac{P\sigma_n^2}{2} + \sigma_n^4 \tag{B-10}$$

The slope of the S-curve can now be found by taking the first derivative of the average error signal with respect to ϕ_{sc}, and afterwards setting $\phi_{sc} = 0$. Accordingly, the slopes of the conventional and modified subcarrier loop are given as

$$K^I_{g,sc} = \frac{1}{\pi}P \tag{B-11}$$

$$K^{IQ}_{g,sc} = \frac{2}{\pi}P \tag{B-12}$$

Note the slope of the IQ-arm is identical to the slope of the I-arm when the carrier is locked [5]. Assuming linear theory, the loop SNR for the subcarrier loop is given as

$$\rho_{sc} = \frac{1}{2B_{sc}T}\frac{K^2_g}{\sigma^2_N} \tag{B-13}$$

where B_L is the one-sided noise bandwidth of the loop. Simplifying, the I- and IQ-arm loop SNR's are respectively given as

$$\rho^I_{sc} = \left(\frac{2}{\pi}\right)^2 \frac{P/N_0}{2B_L W_{sc}}\left(1 + \frac{1}{PT/N_0}\right)^{-1} \tag{B-14}$$

$$\rho^{IQ}_{sc} = \left(\frac{2}{\pi}\right)^2 \frac{P/N_0}{B_{sc}W_{sc}}\left(1 + \frac{1}{PT/N_0}\right)^{-1} \tag{B-15}$$

For comparison, the I-arm loop SNR when the carrier is locked is given in Eq. (10). Figure B-3 illustrates the subcarrier loop SNR's when the I-arm, IQ-arm, and the I-arm with the carrier locked are used. For low-symbol SNR's, the I-arm has a loop SNR that is 6 dB lower than when the carrier is locked. Using the IQ-arm recovers 3 of the 6 dB, but at the expense of more hardware. At high-symbol SNR's, the performance of the IQ-arm is identical to the I-arm when the carrier is locked.

The behavior of the I- and IQ-arm for the subcarrier loop is investigated when the carrier is actually locked. For the I-arm, the subcarrier is normalized by a slope that is less than the actual operating slope. Consequently, the operating bandwidth of the loop is actually narrower than the one specified. Fortunately, the subcarrier is normalized by the correct slope for the IQ-arm .

II. Digital Data Transition Tracking Loop SNR Performance

Similar to the subcarrier loop, the conventional digital data transition tracking loop (DTTL) shown in Fig. B-4 will be modified to utilize both the I and Q channels as depicted in Fig. B-5. Assuming perfect subcarrier demodulation, the I and Q components for CSC are given as

$$I_k = \sqrt{P}d_k \cos(\phi_c) + n^I_k \tag{B-16}$$

$$Q_k = \sqrt{P}d_k \sin(\phi_c) + n^Q_k \tag{B-17}$$

where n^I_k and n^Q_k are independent Gaussian random variables with variance $\sigma^2_n = N_0/2T$, and $\phi_c = 2\pi\Delta f_c + \theta_c$ is the difference between the predicted and actual IF carrier frequency.

The performance of the DTTL has been derived in [6] assuming the carrier is locked ($\phi_c = 0$). When this is not the case, as in CSC, the loop suffers degradation; the objective is to quantify the decrease in performance for both

the conventional and the modified DTTL. This analysis closely follows that of [6], except that the data are modulated by a slowly varying cosine function. Assuming the equivalent mathematical model of the DTTL in terms of a phase-locked loop, all the relevant parameters (slope of the S-curve and normalized equivalent noise spectrum) are derived conditioned on ϕ_c. Afterwards, these parameters are averaged over ϕ_c assuming ϕ_c is uniformly distributed from $-\pi$ to π.

The normalized mean of the error signal e_k conditioned on the normalized timing error λ (in cycles) and the carrier predict error ϕ_c is the normalized phase-detector characteristic $g_n(\lambda, \phi_c)$ commonly termed the loop S-curve. Following similar steps as in [6], $g_n^I(\lambda, \phi_c)$ and $g_n^{IQ}(\lambda, \phi_c)$, the S-curves of the conventional and the modified DTTL, are respectively given as

$$g_n^I(\lambda, \phi_c) = \lambda \ |\cos (\phi_c)| \ \text{erf} \ (B) - \frac{W_{sy} - 2\lambda}{8} \ |\cos (\phi_c)| \ [\text{erf} \ (A) - \text{erf} \ (B)] \tag{B-18}$$

$$g_n^{IQ}(\lambda, \phi_c) = \lambda \ |\cos (\phi_c)| \ \text{erf} \ (B) + \lambda \ |\sin (\phi_c)| \ \text{erf} \ (B') - \frac{W_{sy} - 2\lambda}{8} \ |\cos (\phi_c)| \ [\ \text{erf} \ (A) - \text{erf} \ (B)]$$

$$- \frac{w - 2\lambda}{8} \ |\sin (\phi_c)| \ [\ \text{erf} \ (A') - \text{erf} \ (B')] \tag{B-19}$$

where $A = \sqrt{E_s/N_0}|\cos \phi_c|$, $A' = \sqrt{E_s/N_0}|\sin \phi_c|$, $B = \sqrt{E_s/N_0}(1-2\lambda) \ |\cos \phi_c|$, and $B' = \sqrt{E_s/N_0}(1-2\lambda) \ |\sin \phi_c|$. To compute, the S-curve conditioned only on λ, $g_n^I(\lambda, \phi_c)$ and $g_n^{IQ}(\lambda, \phi_c)$ are numerically integrated over ϕ_c assuming uniform distribution. Setting ϕ_c to zero in Eq. (B-18) results in the same S-curve as that in [6].

The first derivative of the S-curve at $\lambda = 0$ is given as

$$K_{g,sy}^I(\phi_c) = |\cos (\phi_c)| \ \text{erf} \ (A) - \frac{W_{sy}}{2} \ \cos^2 (\phi_c)\sqrt{\frac{E_s}{N_0\pi}} \ \exp \ (-A^2) \tag{B-20}$$

$$K_{g,sy}^{IQ}(\phi_c) = |\cos (\phi_c)| \ \text{erf} \ (A) - \frac{W_{sy}}{2} \ \cos^2 (\phi_c)\sqrt{\frac{E_s}{\pi}} \ \exp \ (-A^2)$$

$$+ |\sin (\phi_c)| \ \text{erf} \ (A') - \frac{W_{sy}}{2} \ \sin^2 (\phi_c)\sqrt{\frac{E_s}{\pi}} \ \exp \ (-A'^2) \tag{B-21}$$

where $K_{g,sy}^I(\phi_c)$ and $K_{g,sy}^{IQ}(\phi_c)$ denote the slope of the S-curve for the conventional and modified DTTL conditioned on ϕ_c, respectively. Numerically integrating over the carrier phase ϕ_c results in the unconditional slopes denoted $K_{g,sy}^I$ and $K_{g,sy}^{IQ}$, respectively.

Setting ϕ_c in Eq. (B-20) to zero results in

$$K_{g,sy} = \text{erf} \ \left(\sqrt{\frac{E_s}{N_0}}\right) - \frac{W_{sy}}{2}\sqrt{\frac{E_s}{N_0\pi}} \ \exp \ \left(-\frac{E_s}{N_0}\right) \tag{B-22}$$

which is identical to the slope given in [6]. Figure B-6 lists the ratio of $K_{g,sy}^I/K_{g,sy}$ and $K_{g,sy}^{IQ}/K_{g,sy}$ for different symbol SNR's and window sizes. At low-symbol SNR, $K_{g,sy}$ and $K_{g,sy}^{IQ}$ are about the same, while $K_{g,sy}^I$ is about twice as large.

Also, the normalized noise spectrum at $\lambda = 0$ can be shown to be

$$h^I(0, \phi_c) = 1 + 0.5 W_{sy} \frac{E_s}{N_0} \cos^2(\phi_c) - \frac{W_{sy}}{2} \left[\frac{1}{\sqrt{\pi}} \exp(-A^2) + \sqrt{\frac{E_s}{N_0}} |\cos(\phi_c)| \operatorname{erf}(A) \right]^2 \qquad \text{(B-23)}$$

$$h^{IQ}(0, \phi_c) = 2 + 0.5 W_{sy} \frac{E_s}{N_0} - \frac{W_{sy}}{2} \left[\frac{1}{\sqrt{\pi}} \exp(-A^2) + \sqrt{\frac{E_s}{N_0}} |\cos(\phi_c)| \operatorname{erf}(A) \right]^2$$

$$- \frac{W_{sy}}{2} \left[\frac{1}{\sqrt{\pi}} \exp(-A'^2) + \sqrt{\frac{E_s}{N_0}} |\sin(\phi_c)| \operatorname{erf}(A') \right]^2 \qquad \text{(B-24)}$$

where $h^I(0, \phi_c)$ and $h^{IQ}(0, \phi_c)$ denote the normalized noise spectrum for the conventional and modified DTTL conditioned on ϕ_c, respectively. Numerically integrating over the carrier phase, ϕ_c, results in the unconditional normalized noise spectrum denoted as $h^I(0)$ and $h^{IQ}(0)$, respectively. Setting ϕ_c in Eq. (B-23) to zero results in

$$h(0) = 1 + 0.5 W_{sy} \frac{E_s}{N_0} - \frac{W_{sy}}{2} \left[\frac{1}{\sqrt{\pi}} \exp\left(-\frac{E_s}{N_0}\right) + \sqrt{R_s} \operatorname{erf}\left(\sqrt{\frac{E_s}{N_0}}\right) \right]^2 \qquad \text{(B-25)}$$

which is the same as the normalized noise spectrum given in [6]. Figure B-7 lists values of $h(0)$, $h^I(0)$, and $h^{IQ}(0)$ for different symbol SNR's at $W_{sy} = 1$. It is evident that $h(0)$ is slightly greater than $h^I(0)$ but significantly less than $h^{IQ}(0)$.

Assuming linear theory, the loop SNR for the DTTL is given as [6]

$$\rho_{sy} = \frac{1}{2\pi^2} \frac{P}{N_0 W_{sy} B_{sy}} \mathcal{L} \qquad \text{(B-26)}$$

where $\mathcal{L} = K_{g,sy}^2/h(0)$. Furthermore, the loop SNR for the conventional and modified DTTL, denoted ρ_{sy}^I and ρ_{sy}^{IQ}, are found by normalizing Eq. (B-26) by $\mathcal{L}^I = (K_{g,sy}^I)^2/h^I(0)$ or $\mathcal{L}^{IQ} = (K_{g,sy}^{IQ})^2/h^{IQ}(0)$, respectively. Figure B-8 illustrates the loop SNR of the DTTL using the I-arm, IQ-arm, and I-arm when the carrier is locked. At low-symbol SNR, it is clear that using only the I-arm reduces the loop SNR by 6 dB compared to the case when the carrier is locked, and utilizing the IQ-arm recovers 3 of the 6 dB.

The behavior of the I- and IQ-arm for symbol loop is investigated when the carrier is actually locked. For the I-arm, the symbol loop is normalized by a slope that is less than the actual operating slope, as shown in Fig. B-6. Consequently, the operating bandwidth of the loop is actually narrower than the one specified. Fortunately, at low-symbol SNR, the symbol loop is normalized by the correct slope for the IQ-arm. For high-symbol SNR, however, the symbol loop for the IQ-arm is normalized by a slope that is greater than the actual operating slope and, consequently, the operating bandwidth of the loop is actually wider that the one specified.
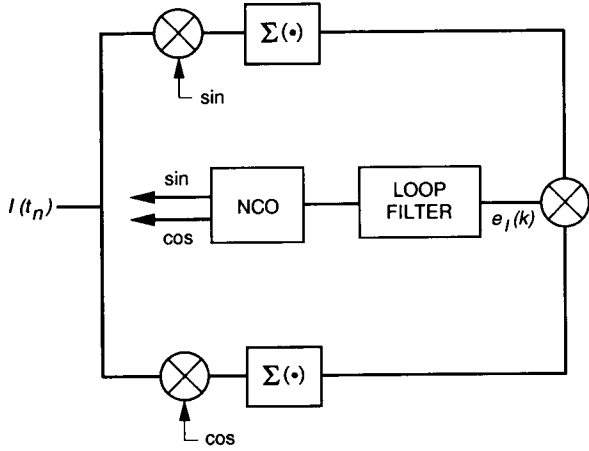
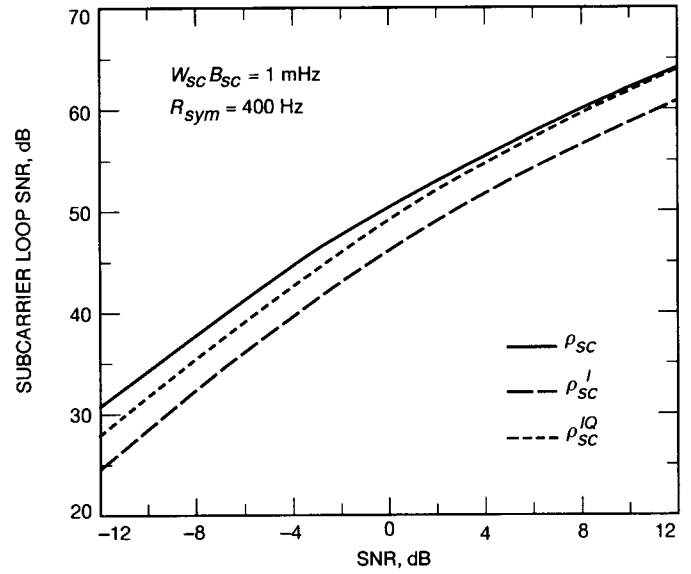Fig. B-1. The unmodified subcarrier loop.

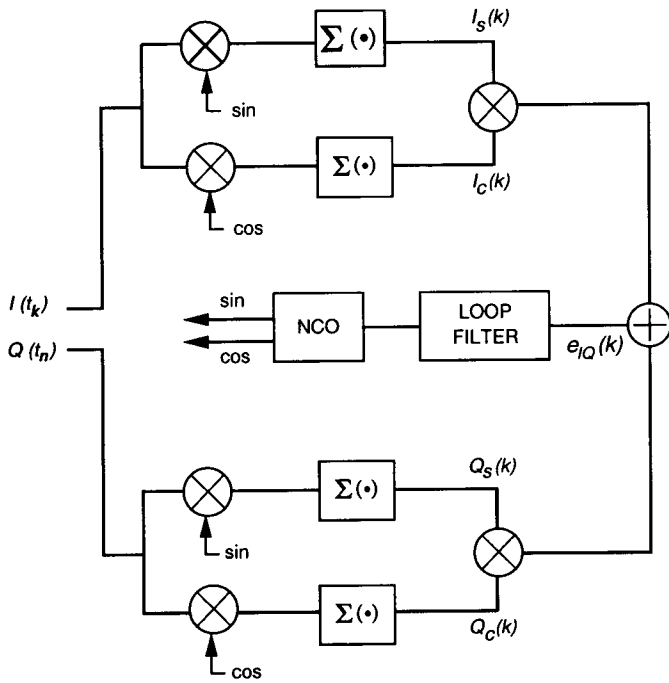Fig. B-3. Subcarrier loop SNR versus symbol SNR.

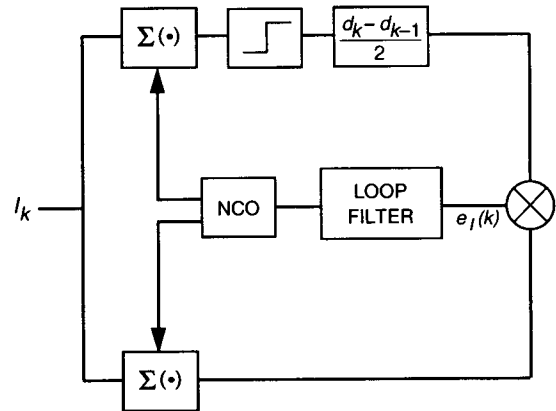Fig. B-2. The modified subcarrier loop.

Fig. B-4. The unmodified digital data transition
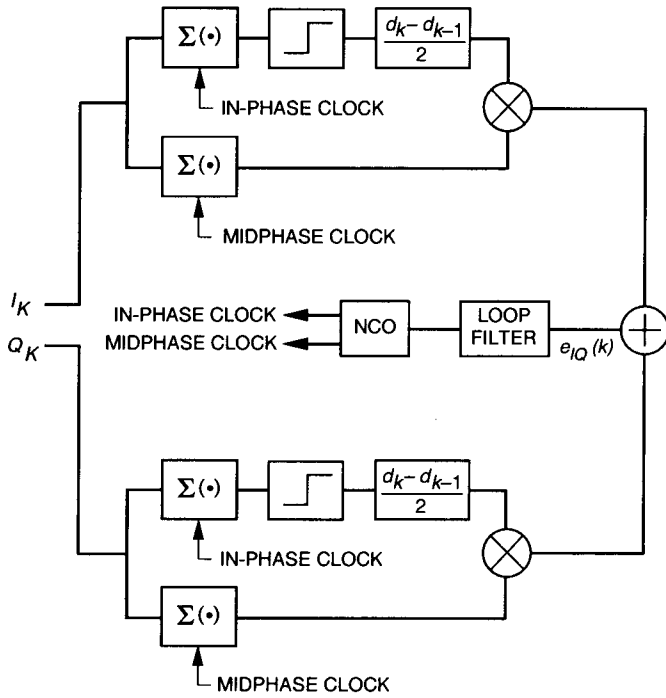tracking loop (DTTL).

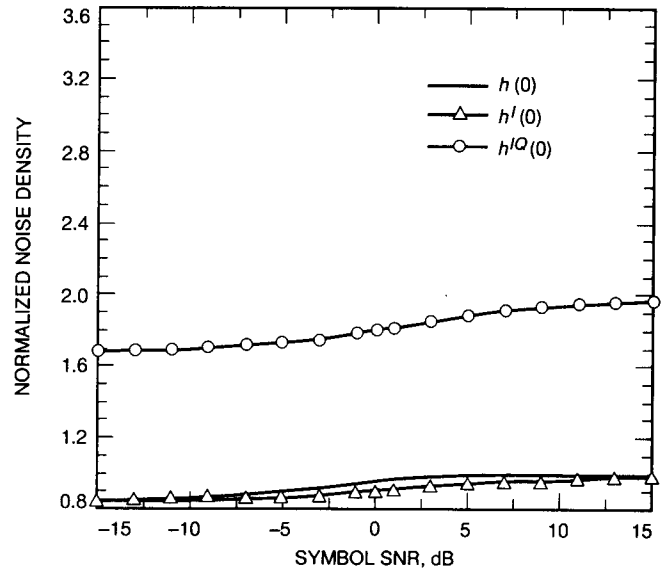Fig. B-5. The modified digital data transition tracking loop.

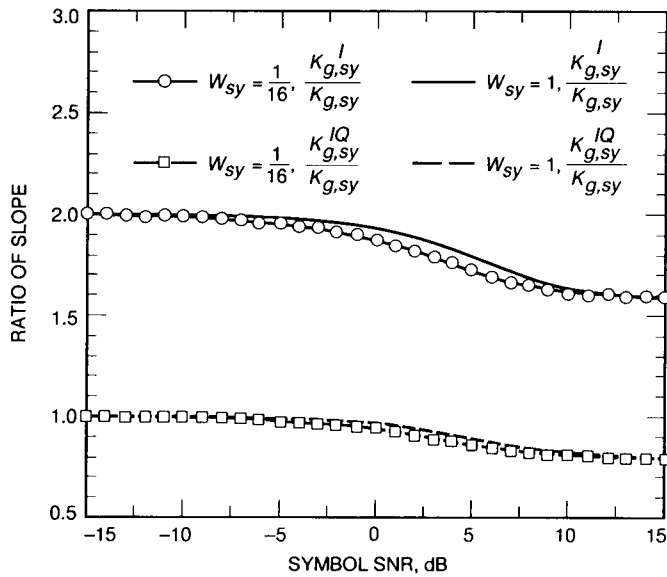Fig. B-7. DTTL symbol SNR versus normalized noise density.

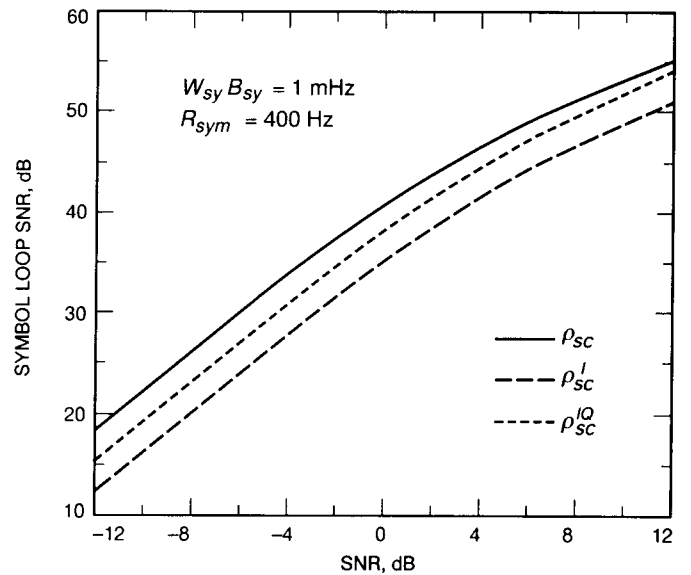Fig. B-6. DTTL symbol versus ratio of slope.

Fig. B-8. Symbol loop SNR versus symbol SNR.

Appendix C

Derivation of Equations

I. Derivation of Eq. (45)

Substituting Eq. (41) into Eq. (43) yields

$$\tilde{z}_k = \begin{cases} \sum_{n=1}^{L} \beta_n \sqrt{P_n} C_{sc_n} d_k e^{[j(\Delta\omega_c t_k + \Delta\phi_{n1})]} + \tilde{n}_{k,n} e^{[-j(\hat{\theta}_{n1})]} & d = d_{k-1} \\ \sum_{n=1}^{L} \beta_n \sqrt{P_n} C_{sc_n} \left(1 - \frac{|\phi_{sy_n}|}{\pi}\right) d_k e^{[j(\Delta\omega_c t_k + \Delta\phi_{n1})]} + \tilde{n}_{k,n} e^{[-j(\hat{\theta}_{n1})]} & d_k \neq d_{k-1} \end{cases} \tag{C-1}$$

where $\Delta\phi_{n1} = \theta_{n1} - \hat{\theta}_{n1}$ and all other symbols are defined in Eq. (41). The conditional combined power, denoted P', in Eq. (45) is found by deriving the conditional mean of $\tilde{z}_k$, i.e.,

$$P' = E(\tilde{z}_k/\phi_{sc_n}, \phi_{sy_n}, \Delta\phi_{n1}) E^*(\tilde{z}_k/\phi_{sc_m}, \phi_{sy_m}, \Delta\phi_{m1})$$

$$= \begin{cases} \sum_{n=1}^{L} \sum_{m=1}^{L} \beta_n \beta_m \sqrt{P_n} \sqrt{P_m} C_{sc_n} C_{sc_m} e^{j[\Delta\phi_{n1} - \Delta\phi_{m1}]} & d_k = d_{k-1} \\ \sum_{n=1}^{L} \sum_{m=1}^{L} \beta_n \beta_m \sqrt{P_n} \sqrt{P_m} C_{sc_n} C_{sc_m} \left(1 - \frac{|\phi_{sy_n}|}{\pi}\right) \left(1 - \frac{|\phi_{sy_m}|}{\pi}\right) e^{j[\Delta\phi_{n1} - \Delta\phi_{m1}]} & d_k \neq d_{k-1} \end{cases} \tag{C-2}$$

which simplifies to Eq. (47). In addition, the phase $\theta_{\tilde{z}}$ in Eq. (45) is given as

$$\theta_{\tilde{z}} = \begin{cases} \tan^{-1} \dfrac{\left(\sum_{n=1}^{L} \beta_n \sqrt{P_n} C_{sc_n} \cos\left(\Delta\omega_c t_k + \Delta\phi_{n1}\right)\right)}{\left(\sum_{n=1}^{L} \beta_n \sqrt{P_n} C_{sc_n} \sin\left(\Delta\omega_c t_k + \Delta\phi_{n1}\right)\right)} & d_k = d_{k-1} \\[6ex] \tan^{-1} \dfrac{\left(\sum_{n=1}^{L} \beta_n \sqrt{P_n} C_{sc_n} \left(1 - \frac{|\phi_{sy_n}|}{\pi}\right) \cos\left(\Delta\omega_c t_k + \Delta\phi_{n1}\right)\right)}{\left(\sum_{n=1}^{L} \beta_n \sqrt{P_n} C_{sc_n} \left(1 - \frac{|\phi_{sy_n}|}{\pi}\right) \sin\left(\Delta\omega_c t_k + \Delta\phi_{n1}\right)\right)} & d_k \neq d_{k-1} \end{cases} \tag{C-3}$$

II. Derivation of Eq. (51)

Let C_{sy_n} be the signal reduction function due to symbol timing errors in the nth symbol synchronization loop. Then the nth matched filter output in Eq. (41) can be rewritten as

$$\tilde{v}_{k,n} = \sqrt{P_n} C_{sc_n} C_{sy_n} d_k e^{[j(\Delta\omega_c t_k + \theta_{n1})]} + \tilde{n}_{k,n} \tag{C-4}$$

where

$$C_{sy_n} = \begin{cases} 1 & d_k = d_{k-1} \\ \left(1 - \frac{|\phi_{sy_n}|}{\pi}\right) & d_k \neq d_{k-1} \end{cases} \tag{C-5}$$

The relative phase difference between antenna n and the reference antenna is estimated by performing the correlation operation shown in Fig. 2(b). Assuming perfect time alignment, the correlation output $\tilde{x}$ is given as

$$\tilde{x} = \sum_{k=1}^{N} \tilde{v}_{k,n} \tilde{v}_{k,1}^* \tag{C-6}$$

where $N = T_c/T$ is the number of symbols used in the correlation. The correlation time and symbol time are respectively denoted as T_c and T. Substituting the expressions for $\tilde{v}_{k,n}$ and $\tilde{v}_{k,1}^*$ into Eq. (A-6) yields

$$\tilde{x} = \sqrt{P_1 P_n} C_{sc_1} C_{sc_n} C_{sy_1} C_{sy_n} e^{j(\theta_{n1})} + n_{\tilde{x}} \tag{C-7}$$

where

$$\text{Var}(n_{\tilde{x}}) = 2P_1 \overline{C_{sc_1}^2}\, \overline{C_{sy_1}^2}\, \frac{N_{0n}}{2T_c} + 2P_n \overline{C_{sc_n}^2}\, \overline{C_{sy_n}^2}\, \frac{N_{01}}{2T_c} + 2\frac{N_{01} N_{0n}}{2T T_c} \tag{C-8}$$

Using the definition of SNR for complex signals as defined in Eq. (30), the correlator SNR between antenna n and antenna 1 for CSC is given as

$$SNR_{n1,csc} = \frac{\sqrt{P_1 P_n}\, \overline{C_{sc_1}}\, \overline{C_{sc_n}}\, \overline{C_{sy_1}}\, \overline{C_{sy_n}}}{2P_1 \overline{C_{sc_1}^2}\, \overline{C_{sy_1}^2}\, \frac{N_{0n}}{2T_c} + 2P_n \overline{C_{sc_n}^2}\, \overline{C_{sy_n}^2}\, \frac{N_{01}}{2T_c} + 2\frac{N_{01} N_{0n}}{2T T_c}} \tag{C-9}$$

and simplifying yields Eq. (51).